

JOURNAL OF NEW TECHNOLOGIES IN ENVIRONMENTAL SCIENCE

No. 4 Vol. 2 ISSN 2544-7017 www.jntes.tu.kielce.pl Kielce University of Technology

CONTENTS

Taras V. DYKUN, Lubov. I. HAIEVA, Fedir V. KOZAK, Yaroslav M. DEMIANCHUK BIOGAS AS AN ALTERNATIVE FUEL FOR AUTOMOTIVE TRANSPORT IN MOUNTAIN AREAS	149
Igor I. PALIYCHYK DETERMINING OF STRESS-STRAIN STATE OF THE CASING STRING ACCORDING TO THE DIRECTIONAL SURVEY DATA DURING THE WELLBORE CONSTRUCTION	156
Tatiana KUGAEVSKA, Vladimir SHULGIN PROCESSES OF MASS TRANSFER IN PERIOD LOADING CHAMBER OF CONCRETE PRODUCTS	168
Anatolij M. PAVLENKO, Andrii CHEILYTKO INVESTIGATION OF THE PROCESS OF PORE FORMATION BASED MATERIALS HYDROSILICATES	174
Hanna KOSHLAK THE THERMOPHYSICAL PECULIARITIES HEAT AND MASS TRANSFER INOCULATORS IN MELTS METALS	183
Hanna KOSHLAK THERMAL INSULATION MATERIALS WITH POROUS STRUCTURE	187
Anastasiia PAVLENKO THERMAL CONDUCTIVITY OF THE GAS IN SMALL SPACE	197

Editor-in-Chief:

prof. Anatoliy PAVLENKO – Faculty of Environmental, Geomatic and Energy Engineering, Kielce University of Technology (Poland)

Associate Editors:

prof. Lidia DĄBEK – Faculty of Environmental, Geomatic and Energy Engineering, Kielce University of Technology (Poland)

prof. Łukasz ORMAN – Kielce University of Technology (Poland)

Secretary of the Editor Board:

prof. Hanna KOSHLAK – Ivano-Frankivsk National Technical University of Oil and Gas (Ukraine)

International Advisory Board:

prof. Jerzy Z. PIOTROWSKI – Kielce University of Technology (Poland), Chairmans

prof. Lidia DĄBEK – Kielce University of Technology (Poland)

prof. Iosyf MYSAK – Lviv Polytechnic National University (Ukraine)

prof. Alexander SZKAROWSKI – Koszalin University of Technology (Poland)

prof. Jarosław GAWDZIK – Kielce University of Technology (Poland)

prof. Mark BOMBERG – McMaster University (Canada)

prof. Jan BUJNAK – University of Žilina (Slovakia)

prof. Łukasz ORMAN – Kielce University of Technology (Poland)

prof. Wiesława GŁODKOWSKA – Koszalin University of Technology (Poland)

prof. Ejub. DZAFEROVIC – International University of Sarajevo (Bosnia-Herzegovina)

prof. Hanna KOSHLAK – Ivano-Frankivsk National Technical University of Oil and Gas (Ukraine)

prof. Oleg MANDRYK – Ivano-Frankivsk National Technical University of Oil and Gas (Ukraine)

prof. Andrej KAPJOR – University of Zilina (Slovakia)

prof. Ibragimow SERDAR – International University of Oil and Gas (Turkmenistan)

prof. Valerii DESHKO – National Technical University of Ukraine “Igor Sikorsky Kyiv Polytechnic Institute” (Ukraine)

prof. Zhang LEI – Faculty of Thermal Engineering, CUPB University of Oil and Gas (China)

prof. Vladimir KUTOVOY – National Science Center Kharkov Institute of Physics and Technology (Ukraine)

prof. Milan MALCHO – University of Žilina (Slovakia)

prof. Anton GANZA – National Technical University of Ukraine “Kharkiv Polytechnic Institute” (Ukraine)

prof. Indira BULJUBAŠIĆ – University of Tuzla (Bosnia-Herzegovina)

prof. Jacek PIEKARSKI – Koszalin University of Technology (Poland)

prof. Alexander M. GRIMITLIN – Saint Petersburg State University of Architecture and Civil Engineering, Association "ABOK NORTH-WEST" Saint-Petersburg (Russia)

prof. Malik G. ZIGANSHIN – Kazan state power engineering university (Russia)

www.jntes.tu.kielce.pl

jntes@tu.kielce.pl

The quarterly printed issues of Journal of New Technologies in Environmental Science are their original versions.

The Journal published by the Kielce University of Technology.

ISSN 2544-7017

© Copyright by Wydawnictwo Politechniki Świętokrzyskiej, 2018

Taras V. DYKUN, Lubov. I. HAIEVA
Fedir V. KOZAK, Yaroslav M. DEMIANCHUK

Ivano-Frankivsk National Technical University of Oil and Gas, Ukraine

BIOGAS AS AN ALTERNATIVE FUEL FOR AUTOMOTIVE TRANSPORT IN MOUNTAIN AREAS

Abstract: *The importance of the problem of effective use of traditional energy sources and the search for alternative resources is beyond doubt. However, nowadays Ukraine does not fully use the potential of low-calorie gases, in particular, biogas, produced by agriculture and industry in large quantities. The number of available domestic installations for the disposal of this gas is negligible although a great number of developed countries have thousands of such facilities.*

One of the most advantageous sources of energy is biogas produced out of biological waste from communal and agricultural dumps – landfill sites for waste disposal. It is meanwhile burnt in flares or emitted into the atmosphere contaminating it heavily. The level of biogas used as a fuel in automotive internal combustion engines is very low. However, replacing gasoline with biogas results in engine power reduction and fuel consumption increase. This should be taken into account when operating cars in mountainous areas where atmospheric pressure and temperature are lower.

Keywords: *biogas, efficiency, the heat of combustion, atmospheric pressure, temperature, power, specific consumption.*

Introduction

Biogas is a gas formed by microbiological decomposition of organic waste in landfills, swamps, sewage systems, and the like.

Today, the share of renewable energy in the world energy balance is negligible – it accounts for only 14%, with biomass contribution being 1.2%. Yet, as practice proves, even slight fluctuations in energy resource markets result in significant energy price increases. Therefore, the role of alternative energy in the markets will only grow. The world biomass energy is up to 13% in the structure of alternative energy. According to recent research, by 2040 the share of renewable energy sources will reach 47.7% and biomass will contribute to 23.8% [1].

The problem of mountainous condition impact on performance indicators of automobile engines running on biogas in Ukraine and in the world is not paid enough attention to.

Exploitation of cars on mountain roads in the Carpathian region is rather difficult at altitudes of 1000÷2000 m above sea level with ascents and descents reaching 12%, the length of sections ranging from 10 km to 15 km.

The higher is the elevation above the sea level, the lower is atmospheric pressure, air density, and temperature, which affect the filling of the car engine cylinder. Concurrently, air leakage and low speeds on steep climbs result in reducing the engine cooling rate. At the same time, the work of engines on the combustible mixture in question and the movement for the most part on the lower gears leads to engine overheating, and the boiling temperature of the coolant gets reduced in the mountains.

Analysis of modern foreign and domestic data

According to the data presented in [2], there is a certain dependence of the change in atmospheric pressure and ambient temperature on the altitude which is shown in table 1.

TABLE 1. Basic environmental indicators depending on altitude

Position	Altitude, m	Atmospheric pressure, kPa	Temperature, °C
1	0	101.3	20
2	1000	89.9	13.5
3	2000	79.5	7
4	3000	70.1	0.5

The **purpose** of the article is twofold: 1) to analyze the possibility and features of the use of biogas as a fuel for internal combustion engines in mountainous conditions; 2) to investigate the influence of separate parameters of the environment in mountainous conditions on the work of internal combustion engines, their technical and operational indicators.

International experience

Biogas technologies are developing at a fast pace. According to the International Bioenergy Journal, 80% of the biogas potential is contained in agricultural raw materials and 10÷11% in industrial and municipal waste. Now Germany ranks first in Europe in the number of biogas plants: in **2010** there were more than 9000 of them. 7% of the biogas produced by these plants is supplied to gas pipelines, the rest is used for the needs of the producer. Denmark is a leader in terms of biogas application. There this type of fuel accounts for almost 20% of the total energy consumption of the country.

Twelve European countries (Austria, Czech Republic, Germany, Denmark, Finland, Sweden, Great Britain, Italy, Iceland, Hungary) use biomethane to fuel motors (including its blend with natural gas), as well as to produce heat [3].

There are few examples of biogas technologies in Ukraine. Several biogas projects at Solid Waste Landfills (SWL) in Mariupol, Lviv, Kremenchug, Lugansk, Kyiv, as well as at Bortnitsky Sewage Treatment Plant of (Kyiv). The project implemented by the LNC Company at Kiev landfill No. 5 proved to be the most successful: the site is equipped with five TEDOM diesel biogas engine with an installed capacity of 177 kW. A vivid example of successful biogas projects concerning the use of biogas for internal combustion engines is the biogas installation "Polygon TPV in the village of Rybne" near the city of Ivano-Frankivsk. 18 boreholes were drilled for biogas production from the landfill, and two gas-fired 330 kW plants were installed to generate electricity. Unfortunately, examples of successful biogas use for automotive internal combustion engines, apart from primitive farmer projects, can be hardly found in Ukraine.

Compared with traditional fuels, biogas has the following advantages:

- It is made from biological raw materials, hence its production and incineration are part of the natural cycle of carbon, which does not cause gas accumulation in the atmosphere and does not result in the greenhouse effect. Environmental damage from organic waste collection systems is decreasing. An ecologically close energy system is provided.
- Biogas is a renewable energy source; in fact, it will never get exhausted if compared with petroleum which is anticipated to get exhausted in no more than 50 years [4].
- Biogas is produced close to the consumer, the raw material for its production is also located not far from the factories and there is no need to transport gas over long distances.

The average component composition of biogas is given in table 2.

TABLE 2. Component composition of biogas

No.	Component	Content, % volume
1	Methane (CH ₄)	50÷75
2	Carbon dioxide (CO ₂)	25÷50
3	Hydrogen (H ₂)	0÷1.0
4	Hydrogen sulfide (H ₂ S)	0÷3.0
5	Nitrogen (N ₂)	0÷10.1
6	Oxygen (O ₂)	0÷2.0

Availability of biogas in hydrogen sulfide is a rather negative factor since hydrogen sulfide reacts with most metals and can cause corrosion of some parts of internal combustion engines, reservoirs, and tanks. Therefore, the issue of cleaning biogas is of great importance.

In comparison with traditional automobile fuels, a major disadvantage of biogas is a low concentration of energy from its combustion, which leads to a decrease in the efficiency of the engine, effective power, and increased fuel consumption.

Knowing the component composition of biogas by the Mendeleev formula, we can calculate the biogas combustion heat Q_H :

$$Q_H = 128 \cdot CO + 108 \cdot H_2 + 234 \cdot H_2S + 339 \cdot CH_4 + 589 \cdot C_nH_m \quad [kJ/m^3] \quad (1)$$

where CO, H₂, H₂S, CH₄, C_nH_m are amounts of individual components in gaseous fuel, % volume under normal conditions.

According to formula (2), combustion heat of gas mixtures is calculated as

$$Q_{n.c.} = \frac{Q_H \cdot \eta}{1 + \alpha L_0} \quad (2)$$

where:

η – a coefficient of combustion completeness;

L_0 – the theoretically calculated volume of air necessary to combust 1 m³ of fuel under normal conditions.

Our calculations show that when the air excess coefficient $\alpha = 1$, the values of the lower heat for the Opel-Vectra engine are as follows:

- for the gas-air mixture – $Q_H = 3739$ kJ/m³,
- for the air-gas mixture – $Q_H = 3404$ kJ/m³,
- for the biogas-air mixture (with CH₄ content = 62%) – $Q_H = 2168$ kJ/m³.

Compared with the standard fuel, reduction of the specific heat of combustion of 1 m³ of the combustible mixture with natural gas CH₄ is 8.7%, of biogas is 42.1%, and of the mixture of biogas and 30% CH₄ is 15.25%. That is, one of the options for improving the performance of internal combustion engines is to mix natural gas with biogas. The lower heat of combustion of such a mixture varies according to the graph shown in figure 1.

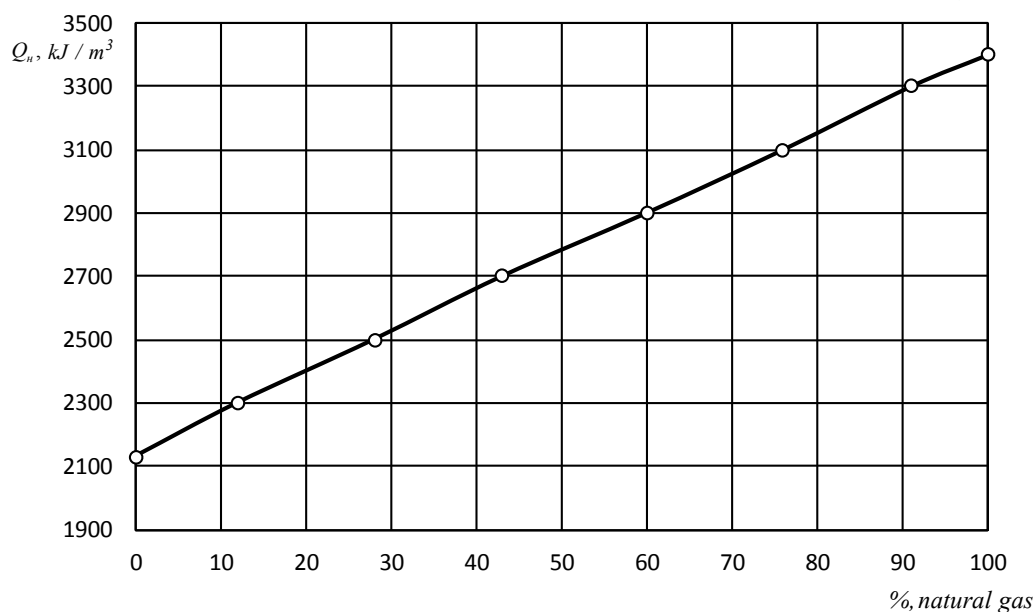


FIGURE 1. Lower heat of combustion of gas mixtures of CH_4 and biogas

Discussion

The research was carried out on the engine ZMZ-5234 and ZIL-130. The necessary calculations were made by using the software complex designed for calculation and optimization of internal combustion engines "Diesel-PC" [5] was used.

The main technical and operational indices of automobile engines are the effective power N_e , torque M_k , specific effective g_e and hourly fuel consumption G_T

$$N_e = \frac{P_e \cdot V_h \cdot n \cdot i}{30 \cdot \tau} \quad [\text{kWt}] \quad (3)$$

where

V_h – the operating volume of the engine, l;

n – a number of revolutions, rpm;

i – a number of cylinders;

τ – a stroke of the engine.

$$M_k = \frac{3 \cdot 10^4 \cdot N_e}{\pi \cdot n} \quad [\text{H} \cdot \text{m}] \quad (4)$$

Specific effective fuel consumption is

$$g_e = \frac{G_T}{N_e} \quad \left[\frac{\text{kg}}{\text{kWt} \cdot \text{hr}} \right] \quad (5)$$

where G_T is hourly fuel consumption, g/h.

As a result of analytical studies, the graphs of the dependence of the change in effective power and on the effective specific biogas consumption rate from changes in temperature and changes in atmospheric pressure of the environment were obtained.

These dependences are shown in figures 2-5.

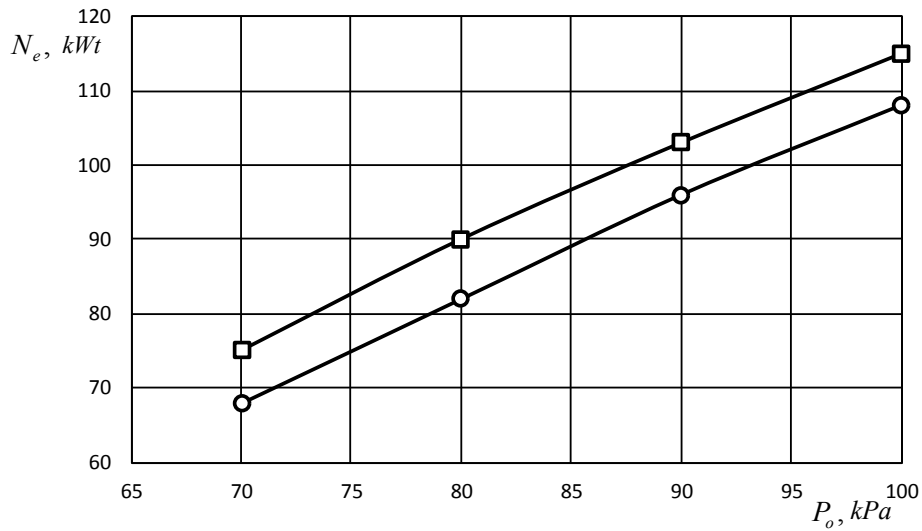


FIGURE 2. Dependence of the effective power change of Engine ZMZ-5234.10 on atmospheric pressure

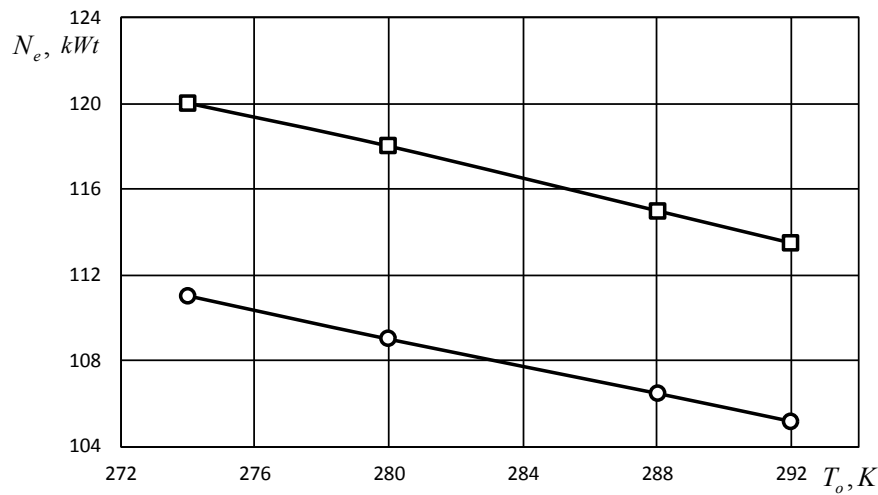


FIGURE 3. Dependence of the effective power change of the Engine ZMZ-5234.10 on the temperature change of the environment

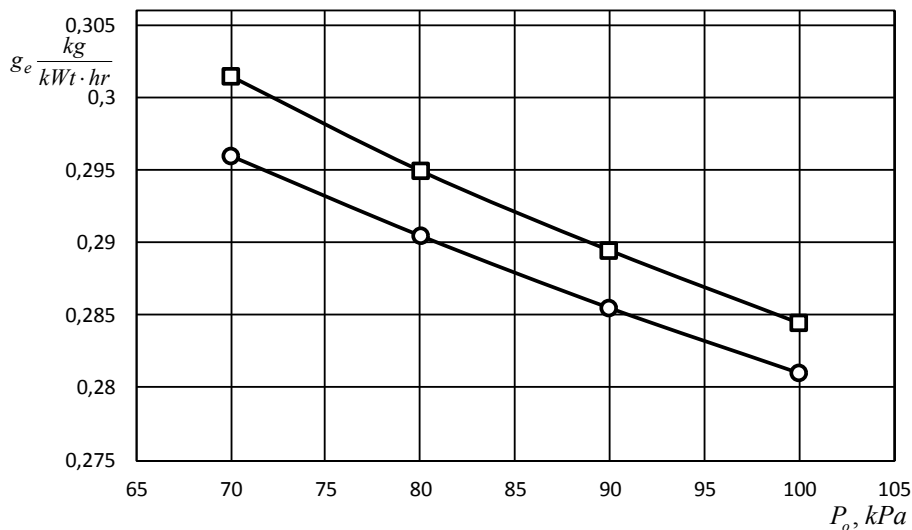


FIGURE 4. The change in the specific effective fuel consumption of Engine ZMZ-5234.10 on the atmospheric pressure change

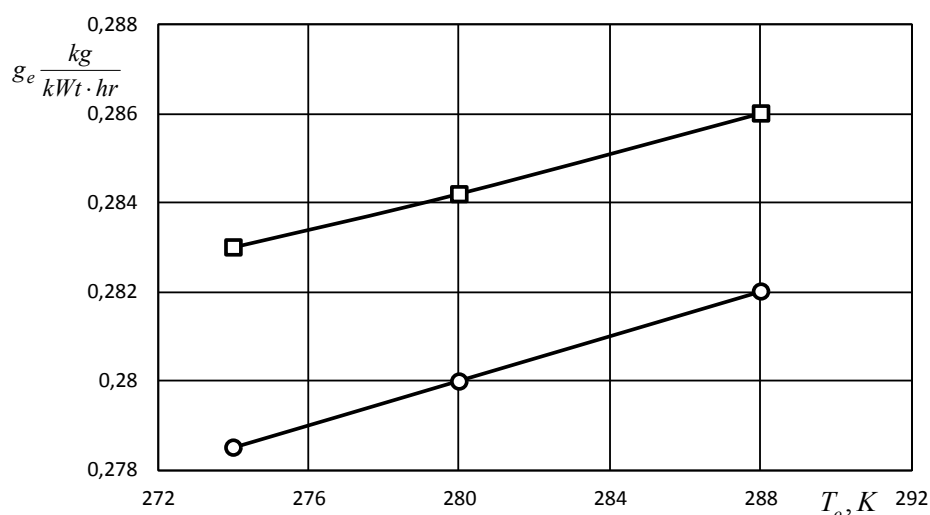


FIGURE 5. The change in the specific effective fuel consumption of Engine ZMZ-5234.10 on the ambient temperature changes

As the study proves, when using biogas as automotive fuel in mountainous conditions with lower atmospheric pressure, the effective power is reduced by 6÷9% compared with gasoline; and the specific effective fuel consumption is increased by 7.3-7.5% depending on the size of the reduced pressure. By reducing the ambient temperature, the effective engine power is reduced by 14÷16% and the specific effective fuel consumption is increased by 14÷20%. The impact of these factors can be reduced by adding natural gas to biogas. How it affects the specific effective fuel consumption in engines is shown in figure 6.

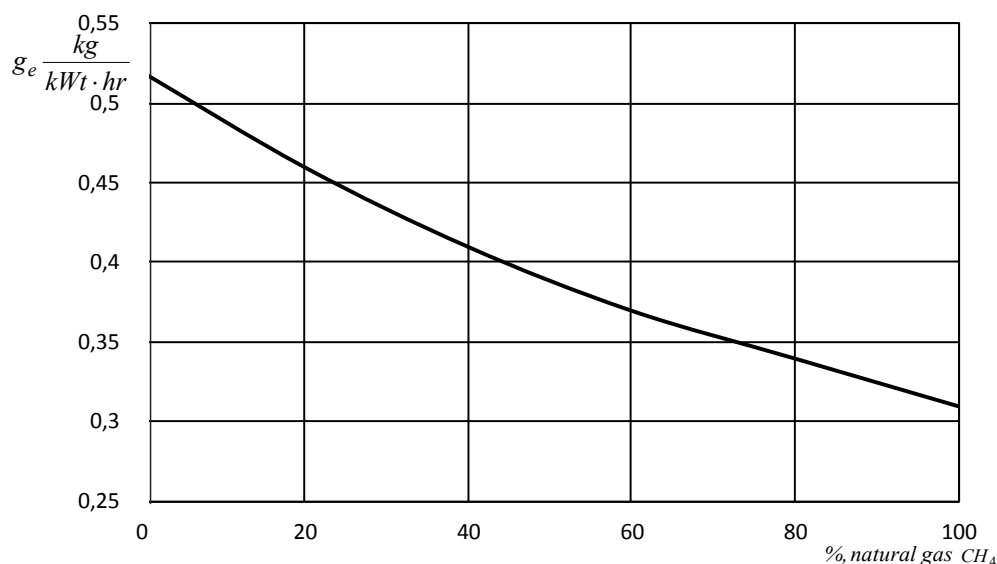


FIGURE 6. Changes of the specific fuel efficiency when adding natural gas

Conclusions

1. The use of biogas for internal combustion engines in mountain conditions may partially solve the problem of fuel shortages. Ukraine has the necessary reserves to do this.
2. Since the lower heat of biogas combustion is by (40÷45)% less than that of conventional petroleum fuels, the capacity and specific effective consumption of fuel used by cars running in mountain conditions are significantly changing. Depending on the ambient temperature, the power is reduced

by 14÷16%, and the specific fuel consumption is increased by 14÷20%. Depending on the altitude, the power is reduced by 6÷9%, and fuel consumption is increased by 7.3-7.5%.

3. It is possible to improve the technical and operational performance of internal combustion engines by blending natural gas and biogas.

References

- [1] International Energy Outlook 2001. U.S. Department of Energy, March 2001 (IEO 2001).
- [2] Tursunov A.A.: *Vlyaniye atmosferno-klymatycheskykh usloviy reliefa mestnosti na effektivnost raboty avtomobylei* (Influence of atmospheric-climatic conditions and terrain on car performance), A.A. Tursunov, M.A. Abdulloev, Problemy transporta Dalnego Vostoka: Sb. Vladivostok 2001, No. 1, pp. 277-279 (in Russian).
- [3] Kuleshov A.S.: *Prohramma rascheta y optymyzatsyy dvyhatelei vnutrenneho shoranyia DYZEL-RK* (Software for calculation and optimization of internal combustion engines DIESEL-RK), A.S. Kuleshov. M: MHTU named after Bauman, 2004, 123 p. (in Russian).
- [4] *Avtomobilni dvyhunyy* (Automobile engines), Abramchuk F.I., Hutarevych Yu.F., Dolhanov K.Ie., Tymchenko I.I. – K: Aristei, 2004, 438 p. (in Ukrainian).
- [5] Biogas. – URL: <http://uk.wikipedia.org/wiki/Biogas>.

Igor I. PALIYCHYK

Ivano-Frankivsk National Technical University of Oil and Gas, Ukraine

DETERMINING OF STRESS-STRAIN STATE OF THE CASING STRING ACCORDING TO THE DIRECTIONAL SURVEY DATA DURING THE WELLBORE CONSTRUCTION

Abstract: *The casing string in the curvilinear borehole is represented as a long elastic rod, for which a non-uniform system of differential equations is constructed and integrated taking into account its own weight and friction. Formulas for the distribution of axial forces and bending moments in the body of the column, as well as the reactions of the walls leading the column to the actual well profile are obtained. To calculate these force factors, a method for numerical integration of inclinometric measurements data and software for numerical analysis of a real well are developed. This technique allows to detect the areas of local increase of the curvature and difficult passage of the curvilinear well and calculate the parameters of the stress-strain state of the casing column in it.*

Keywords: *casing string, curved well, inclinometric measurements, axial force, wall reaction.*

Introduction

The technology of reliable and safe extraction of oil and gas from large depths requires the borehole wall lining by a string of casing. Modern methods of directional and horizontal drilling allow to reach productive layers at a depth of 4÷6 km with a string length of 5÷8 km, while steel pipes have a diameter of only 168÷140 mm with a wall thickness of 10÷12 mm. The main production casing, which connects the wellhead with deposits of hydrocarbons, must be continuous, strong and pressure-tight.

A typical well program includes a vertical section, one or more inclined sections (which provide a large deviation from the vertical one) and a vertical bottom-hole section. The straight-line areas are interconnected by transition curved ones, which are described by the circle arc of a constant radius. When designing, all wells are usually located in one vertical plane.

While drilling there are deviations from the well design profile, which are continuously corrected by technical and technological means. As a result, the area of the real well is not exactly straight or circular arc, but contains local distortions and deviations from the given shape. To establish the real profile of the drilled well, its logging is conducted, during which zenith angle ϑ between the tangent to the curved axis of the well and the vertical is measured. According to the data obtained, an inclinometric table is compiled demonstrating the table dependence of the angle $\vartheta(s)$ from the coordinate s , which is the distance from the earth surface along the curved axis of the well to the specified intersection. Measurements are carried out from the wellhead to the bottom with a certain pitch Δs .

The production casing, lowered into the curved well, enters into force interaction with the wells due to the rigidity of the pipes. Due to the reaction of the walls, the string bends, resembling the profile of the well. As a result, in the pipes body there emerges a complex stress-strain state caused by their bending and axial tension, which greatly affects the reliability and durability of the casing.

Literature review

The work of Yu. Pesliak [1] is devoted to the study of internal stresses in the columns of oil wells. The problem of determining the forces acting on the string of pipes in the well when its shape is given is considered here. To solve it, a system of G. Kirchhoff equations describing the spatial deviations of a long elastic rod, which has a finite bending stiffness, has been used, and its solution in a vector form has been carried out. However, the results in scalar form suitable for engineering calculations are obtained only for the case of a well section, which is curved along a circular arc of a constant radius in one plane, and for a well case, which is presented by a helix with a constant zenith angle and a constant rate of change of the azimuthal angle. In order to determine the axial forces and frictional forces in the case of random deviation of the well, numerical integration is applied on an example of a well with a constant speed of change of the zenith and azimuthal angle to their maximum value of 90° .

In the paper by P. Vyslobitskyi [2] the problem of the advance and bending of the string of pipes in the deviated borehole is considered. For its solution a geometric approach is used to study the force interaction of pipes with well walls. At the same time, the pipe was graphically inscribed into well deviated along the circular arc following several possible, according to the author, schemes of placement of contact points with its walls, in which reactions and frictional forces may occur. The acting forces were determined by the equilibrium equations of the pipe sections between these contact points and the pipe deformation equations, for which the formulas of the small deformations of the cantilever beam were unjustifiably applied. With the general formulation of the problem of bending and casing string drift in the deviated wellbore, a system of differential equations was proposed. The system had to express the bent state of the string, but it does not contain two equations of equilibrium of internal and external forces projections, and therefore it is incomplete and cannot be solved.

Thus, *unresolved remains the problem* of obtaining a closed system of differential equations, which describes the deformation of the string of pipes in a deviated well under their own weight and the reactions of the walls. The solutions of this problem will determine the distribution of axial forces, bending moments and stresses in the body of the column.

Purpose

A long casing string in the well behaves like an elastic, solid rod [1, 3], which has sufficient bending stiffness. It is influenced by a vertical weight j , uniformly distributed along the length, which creates variable axial forces in the body of the column. The column of initially rectilinear pipes in the curvilinear well forcibly receives the geometric shape of its curved axis. This is due to the reaction forces of the well walls, which, together with the weight, act on the column and bend it.

In the first approximation, we consider that the column contacts the well walls along its entire length (we neglect small gaps between the wall and the pipe in comparison with large geometric deviations of the axis from the rectilinear form). Consequently, along with the distributed weight j , a long elastic rod is influenced by the reaction of the walls $f(s)$, distributed by its length according to a certain law, as a result of which it acquires a given form. We assume that the distributed load $f(s)$ is directed along the normal to the curvilinear axis of the rod and is positive if its projection to the horizontal has a positive direction.

The purpose of the work is to develop a method for determining the distribution of axial forces and the reactions of the walls, which, together with their own weight, act on a casing string and make it follow a given wellbore shape. To do this, it is necessary to derive and integrate the system of differential equations of equilibrium of a long elastic rod bent in one plane. According to the obtained results, it is necessary to find expressions of force parameters that describe the stress-deformed state of the casing in a deviated well.

The basic system of differential equations

The analysis has showed that large elastic deformations of the long rod of the unit-value stiffness can be considered for the bend, without losing the universality of the solution [3]. At the same time, the bending moment is numerically equal to the curvature of the rod, and the current force factors differ in size from the estimated ones by the factor EJ (E is the elastic modulus of the material, J is the moment of inertia of the cross-section of the rod).

Let us consider the arc element – the segment of the curved axis of the rod with length ds , at the beginning of which the tangent line is inclined to the vertical under zenith angle ϑ (fig. 1). In this section, the internal axial t and transverse u forces as well as bending moment q are applied.

In the final crosscut of the element, which received an increase in zenith angle $d\vartheta$, the same forces are applied, but with increments dt , du , dq correspondingly, the direction of which must balance the initial ones. The element is also affected by external forces: its weight jds , the reaction of the wall fds and the friction force $k_t f ds$, directed along the axis of the string against its motion (not shown in fig. 1), where k_t is the coefficient of friction. In the equations of equilibrium, discussed below, the sign of friction corresponds to the descent of the string in the well. For the case of lifting a column in the equations and their solutions, the coefficient of friction should be taken with the opposite sign.

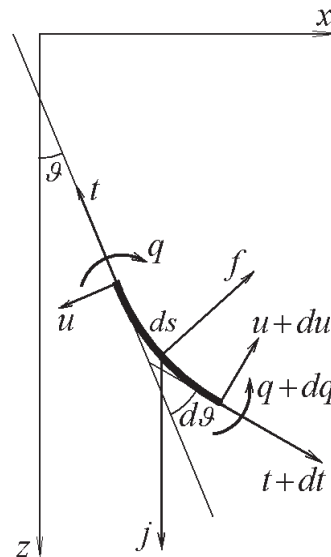


FIGURE 1. Calculation schema of a curved elastic element

Let us project all forces on a normal and tangent line, make an equation of equilibrium of their projections, as well as equations of equilibrium of finite moments and moments of finite forces, and obtain a system of differential equations:

$$\frac{du}{ds} + t \cdot \frac{d\vartheta}{ds} - j \sin \vartheta + f = 0$$

$$\frac{dt}{ds} - u \cdot \frac{d\vartheta}{ds} + j \cos \vartheta - k_t f = 0$$

$$\frac{dq}{ds} + u = 0$$

A similar system describing the bending deformation of a long elastic rod in one plane was obtained in the work of R. Frisch-Fay [4]. However, it did not take into account the reaction of the wall and friction, and was incomplete. In order for the system to have a solution, the fourth equation is required, which

is the kinematic Euler equation. It establishes the connection between the angular deformation of the rod and its curvature q (bending moment)

$$q = \mathcal{G}' = \frac{d\mathcal{G}}{ds} = \frac{1}{R}$$

where R is local radius of curvature; the dot denotes the derivative of s .

Due to this, the system of differential equations becomes closed and has a solution.

Thus, the deformations of casing string, bent due to the deviation of the borehole, are described by a non-uniform system of four differential equations:

$$u' + t \cdot \mathcal{G}' = j \sin \mathcal{G} - f \quad (1)$$

$$t' - u \cdot \mathcal{G}' = -j \cos \mathcal{G} + k_t f \quad (2)$$

$$q' + u = 0 \quad (3)$$

$$\mathcal{G}' - q = 0 \quad (4)$$

As we see, this system (1)-(4) contains three unknown functions t , u and q (which are internal force factors) and an unknown function of the distributed reaction f (which is an external load). The function \mathcal{G} is known due to the inclinometric table of well measurement. It is necessary to solve the inverse problem – having the known load j and the deformations \mathcal{G} given by the shape of the well, it is necessary to determine the unknown internal forces t , u , q and such an external load function f , which creates a given shape of the rod.

Applying the equation (3)-(4), we reduce the system to two equations:

$$t \cdot \mathcal{G}' - \mathcal{G}''' = j \sin \mathcal{G} - f \quad (5)$$

$$t' + \mathcal{G}'' \cdot \mathcal{G}' = -j \cos \mathcal{G} + k_t f \quad (6)$$

The system of differential equations (5)-(6), where the zenith angle function \mathcal{G} is known, contains two unknown functions t and f . According to equation (5) we have

$$f = j \sin \mathcal{G} - t \cdot \mathcal{G}' + \mathcal{G}''' \quad (7)$$

Thus, the problem of determining the distributed reaction of walls f requires the finding of the axial force t . To do this, let us eliminate function f from the system (5)-(6):

$$t' + k_t \mathcal{G}' \cdot t = k_t \mathcal{G}''' - \mathcal{G}' \cdot \mathcal{G}'' + k_t j \sin \mathcal{G} - j \cos \mathcal{G} \quad (8)$$

The resulting differential first-order equation is linear, inhomogeneous and, in general, with variable coefficients. We will study and solve the basic differential equation (8).

Integration of differential equation of axial force

Let us mark the right part (8) in the following way

$$\varphi = k_t \mathcal{G}''' - \mathcal{G}' \cdot \mathcal{G}'' + j(k_t \sin \mathcal{G} - \cos \mathcal{G}) \quad (9)$$

Integration (8) is carried out provided that the coefficient of resistance of the string motion within a single area is constant: $k_t = \text{const}$, $0 < k_t < 1$. Let us solve the Cauchy problem provided that in the established intersection with the coordinate $s=L$, where $z=Z$, $\mathcal{G}=\Theta$ and axial force $t(L)=t_Z$ is applied.

The general solution of the inhomogeneous equation (8) is sought by the Bernoulli method [5] in the form of a product of two functions: $t = v \cdot w$; its substitution in (8) gives

$$\begin{aligned} v' \cdot w + v \cdot w' + k_T g' \cdot v \cdot w &= \varphi \\ (v' + k_T g' \cdot v) \cdot w + v \cdot w' &= \varphi \end{aligned} \quad (10)$$

Since we are looking for one function t , then one of the two product functions can be arbitrary. Choose v such that satisfies the homogeneous equation, formed from the expression in brackets (10) and solution of which we can find by separating the variables:

$$v' + k_T g' \cdot v = 0 \quad (11)$$

$$v = e^{k_T(\Theta - g)} \quad (12)$$

Now let us substitute expressions (11), (12) and (9) into equation (10) and integrate the resulting differential equation:

$$e^{k_t \Theta} (w - c) = k_t \int_L^s e^{k_t g} g''' ds - \int_L^s e^{k_t g} g' g'' ds + j \int_L^s e^{k_t g} (k_t \sin g - \cos g) ds \quad (13)$$

where c is constant of integration.

The first of the integrals containing in (13) is found by integrating the parts:

$$\int_L^s e^{k_t g} g''' ds = \int_{\Theta}^g e^{k_t g} d(g''') = e^{k_t g} g'' - e^{k_t \Theta} g''_{\Theta} - k_t \int_L^s e^{k_t g} g' g'' ds$$

where $g'_{\Theta} = g'(\Theta)$ is the value of the derived function in the intersection, where $g = \Theta$.

Now the first and second integrals of (13) can be combined:

$$k_t \int_L^s e^{k_t g} g''' ds - \int_L^s e^{k_t g} g' g'' ds = k_t e^{k_t \Theta} (e^{k_t(g-\Theta)} g'' - g''_{\Theta}) - (1 + k_t^2) \int_L^s e^{k_t g} g' g'' ds$$

The second of integrals (13) is also integrated by parts:

$$\int_L^s e^{k_t g} g' g'' ds = \frac{1}{2} \int_{\Theta}^g e^{k_t g} d(g'^2) = \frac{e^{k_t \Theta}}{2} (e^{k_t(g-\Theta)} g'^2 - g'^2_{\Theta}) - \frac{k_t}{2} \int_L^s e^{k_t g} g'^3 ds$$

Substituting the resulting integrals in (13), we obtain a function w :

$$w = k_t (e^{k_t(g-\Theta)} g'' - g''_{\Theta}) - \frac{1 + k_t^2}{2} \times \left((e^{k_t(g-\Theta)} g'^2 - g'^2_{\Theta}) - \frac{k_t}{e^{k_t \Theta}} \int_L^s e^{k_t g} g'^3 ds \right) + \frac{j}{e^{k_t \Theta}} \int_L^s e^{k_t g} (k_t \sin g - \cos g) ds + c \quad (14)$$

The product of functions (12) and (14) gives a function t :

$$\begin{aligned} t = e^{k_t(\Theta - g)} w &= k_t (g'' - e^{k_t(\Theta - g)} g''_{\Theta}) - \frac{1 + k_t^2}{2} \times \left((g'^2 - e^{k_t(\Theta - g)} g'^2_{\Theta}) - \frac{k_t}{e^{k_t g}} \int_L^s e^{k_t g} g'^3 ds \right) + \\ &+ \frac{j}{e^{k_T g}} \int_L^s e^{k_T g} (k_T \sin g - \cos g) ds + c e^{k_T(\Theta - g)} \end{aligned}$$

Under the conditions of the Cauchy problem we get $c = t_z$. Consequently, the distribution of the axial force in the body of the column, taking into account the deviation of the well and friction on its walls, has the form

$$t = k_t \left(g'' - g''_{\Theta} e^{k_t(\Theta - \vartheta)} \right) - \frac{1 + k_t^2}{2} \times \left(\left(g'^2 - g'^2_{\Theta} e^{k_t(\Theta - \vartheta)} \right) + \frac{k_t}{e^{k_t \vartheta}} \int_s^L e^{k_t \vartheta} g'^3 ds \right) - \frac{j}{e^{k_t \vartheta}} \int_s^L e^{k_t \vartheta} (k_t \sin \vartheta - \cos \vartheta) ds + t_z e^{k_t(\Theta - \vartheta)} \tag{15}$$

In the expression (15) the direction of integration is changed. Transformations helped to get rid of the second and third derivatives under integrals. The last integral (15) can not be simplified in general case. It can be found in quadratures only for the case of a constant radius of the well curvature when $ds = R d\vartheta$ [3].

Knowing the axial force t (15), one can find a distributed reaction of the well walls by expression (7).

Methods of numerical differentiation and integration of inclinometric table

According to the results of directional survey, that is the table of zenith angles ϑ , measured with the interval Δs , a real well profile is constructed. At first, they determine depth gain Δz , horizontal displacement Δx from the vertical axis of the well in the directional drilling, lateral deviation Δy from the directional orientation:

$$\begin{aligned} \Delta z_n &= \Delta s_n \cos \vartheta_n \\ \Delta x_n &= \Delta s_n \sin \vartheta_n \cos(A_n - Az) \\ \Delta y_n &= \Delta s_n \sin \vartheta_n \sin(A_n - Az) \end{aligned}$$

where:

- n – sequence number of measurement;
- Δs_n – coordinate gain s of intersection along the deviated wellbore, $\Delta s_n = s_n - s_{n-1}$;
- A_n – measured magnetic azimuth;
- Az – azimuth of directional orientation.

According to calculated gains absolute values of depth Z_n , horizontal displacement X_n and lateral deviation Y_n as the sum of gains are determined:

$$Z_n = \sum_{i=1}^n \Delta z_i, \quad X_n = \sum_{i=1}^n \Delta x_i, \quad Y_n = \sum_{i=1}^n \Delta y_i \tag{16}$$

by which they build a vertical profile and a horizontal well plan.

For a numerical differentiation of a table-defined function, a central scheme is used [6]:

$$d\vartheta_n = \frac{\vartheta_{n+1} - \vartheta_{n-1}}{s_{n+1} - s_{n-1}} \tag{17}$$

where the letter d denotes numerical differentiation.

According to (17), the values of the second d^2 and the third d^3 derivatives can be obtained correspondingly:

$$d2\vartheta_n = \frac{d\vartheta_{n+1} - d\vartheta_{n-1}}{s_{n+1} - s_{n-1}} \quad (18)$$

$$d3\vartheta_n = \frac{d2\vartheta_{n+1} - d2\vartheta_{n-1}}{s_{n+1} - s_{n-1}}$$

Applying the expression (7), the true value of F_n of the distributed response of the well wall in the n -th section is found by the formula:

$$F_n = EJf_n = EJj \sin \vartheta_n - T_n \cdot d\vartheta_n + EJ \cdot d3\vartheta_n \quad (19)$$

where $T_n = EJt_n$ is the actual value of the axial force, which must first be found, defining the integrals in the expression (15).

The numerical integration of tabulated functions is carried out according to the trapezoidal rule [6]. For this, the interval of integration $[s, L]$ is divided into elementary intervals; on each of them, they find the area of the trapezoid, constructed on the ordinates of the function at the edges of the interval. The value of an integral is equal to the sum of the squares of all elementary trapezoids.

For an inclinometric table, for an elementary interval, it is natural to choose the measurement interval Δs , which makes it possible to find the values of the integral functions for the formula (15) at the edges of each interval.

As formula (15) shows, to find the value of the axial force t in the current section s , it is necessary to know its value t_z at the end of the integration interval. The only cross section of the casing, where the axial force is known in advance, is its free end (casing shoe) – here $t_z = 0$. Proceeding from this, the following method of numerical analysis of inclinometric table is developed.

For the integration interval, choose the measurement interval Δs . Then in the current section s_n , which is the beginning of the interval and where you need to find the axial force t_n , one can determine all the values of functions and derivatives necessary for (15). The same values at the end of the interval (when $s=L$ and $\vartheta=\Theta$) are found by the data of the next $(n+1)$ -th measurement.

At the same time, for formula (15) the integral value is equal to the trapezoidal area constructed on the ordinates of the integrands determined according to the n -th and $(n+1)$ -th measurements. The value of the trapezoidal area is found as the product of the interval Δs to the arithmetic mean of the specified ordinates.

Thus, transforming formula (15) and integrals in it according to the proposed method, the real value of the axial force T_n at each step of integration is determined by the formula

$$T_n = \frac{EJ}{e^{k\vartheta_n}} \left[k \left(e^{k\vartheta_n} d2\vartheta_n - e^{k\vartheta_{n+1}} d2\vartheta_{n+1} \right) - \frac{1+k^2}{2} \left(e^{k\vartheta_n} (d\vartheta_n)^2 - e^{k\vartheta_{n+1}} (d\vartheta_{n+1})^2 \right) + \right. \\ \left. + k(s_{n+1} - s_n) \cdot \frac{e^{k\vartheta_n} (d\vartheta_n)^3 + e^{k\vartheta_{n+1}} (d\vartheta_{n+1})^3}{2} \right] + \quad (20)$$

$$+ \frac{EJj}{e^{k\vartheta_n}} \cdot \frac{e^{k\vartheta_n} (\cos \vartheta_n - k \sin \vartheta_n) + e^{k\vartheta_{n+1}} (\cos \vartheta_{n+1} - k \sin \vartheta_{n+1})}{2} \times (s_{n+1} - s_n) + T_{n+1} \frac{e^{k\vartheta_{n+1}}}{e^{k\vartheta_n}}$$

Beginning with the last N -th measurement for which the value $T_N = EJt_z = 0$ is known, according to (20) we find the previous value T_{N-1} , by which we get value T_{N-2} and so on. The determination of the distribution of the axial forces in the body of the pipe occurs from the bottom upwards along the casing from its free end, with the preset value of the axial force for the last measurement.

The design of the casing column is described by setting the diameters D_n of the pipes and the thickness δ_n of their walls at each depth interval according to the well program; consequently we determine the area S_n of the crosscut of the pipes and its moments of inertia J_n .

At each depth interval, we set the mass m_t of one linear meter of the casing pipe, the mass m_m of the collar, the length l_m of the pipes (the distance between the couplings), the mass m_c of the centralizer and the distance l_c between them. Determine the combined mass m_n of the linear meter of the casing column by the formula

$$m_n = m_t + \frac{m_m}{l_m} + \frac{m_c}{l_c} \quad (21)$$

The coefficients of friction are given for each interval of bedding of rocks in accordance with the borehole log. We also set the values of the densities γ_n of the drilling fluid, which is in the well after it was washed out before the casing is lowered. The combined weight j_n of the linear casing meter is calculated by the formula

$$j_n = \frac{9.8(\rho - \gamma_n)}{EJ_n} \cdot \frac{m_n}{\rho} \quad (22)$$

where:

ρ – density of the casing material;

$\frac{m_n}{\rho}$ – the volume of its combined cross-section.

Along the wellbore, we find the values of the axial forces and the reactions of the wall by the formulas (20) and (19). The values of the local radii R_n of the curvature and the internal bending moments M_n are calculated by the formulas:

$$R_n = \frac{1}{d\vartheta_n}, \quad M_n = EJq_n = EJd\vartheta_n \quad (23)$$

To determine the strength of the casing, we must determine the local maximal values of internal stresses in the body of the pipes by the sum of stresses from tension and bending:

$$\sigma_{\max} = \frac{T_n}{S_n} + \frac{|M_n|}{J_n} \frac{D_n}{2} = \frac{T_n}{S_n} + \frac{E D_n}{2|R_n|} \quad (24)$$

The value of the bending moment and the radius of curvature is taken modulo to obtain the maximum stress value in the pipe, regardless of the direction of its bend and the location of the stretched fibers.

The developed numerical analysis program has been tested in a test mode by comparing with the results of analytically found formulas of the axial force t and reaction of walls f for a well section of a constant radius of curvature, taking into account frictional forces [3]. At the same time the error of program calculations was no more than 0.02%.

Results and Discussion

Approbation of the developed methodology is carried out according to the data of the operating well number 170. However, at first the analysis of its program was carried out using theoretical solutions. For this purpose, in the areas from which the real program is made, the following parameters are calculated according to the formulas obtained analytically in [3]: the distribution of axial forces in the initial and final vertical sections; the distribution of axial forces and the reactions of the walls on the

radius of zenith angle buildup, on two inclined rectilinear sections and two radius sections of the zenith angle decline. The values of the radii of curvature and bending moments are calculated according to the formulas (23), the maximum stresses – according to (24). The results of calculations are given in table 1.

TABLE 1. Theoretical characteristics of the well program No. 170

Casing length intervals, m	Characteristics of areas	Diameter D of the string, thickness δ of pipe wall, mm	Zenith angle ϑ , angle gain $\Delta\vartheta$ for 10 m	Reaction $F = E\delta f$ of well wall, kN/m	Radius R of curvature, m	Bending moment $M = E\delta q$, kN/m	Tension jump in the pipe body, MPa
0...1200		168×10.6	0°	0	–	0	–
1200...1350	vertical		0°	0	–	0	+29.2
1350...1650	Zenith angle buildup		$\vartheta = 0...14^\circ.5$ $\Delta\vartheta = 0^\circ.5$	–0.85 –0.66	+1146	+1.83	+12.7 –12.7
1650...2400	inclined	146×10.7	$\vartheta = 14^\circ.5$	+0.077	–	0	–
2400...2480	Zenith angle decline		$\vartheta = 14^\circ.5...13^\circ.7$ $\Delta\vartheta = -0^\circ.1$	+0.19 +0.18	–5730	–0.37	+2.6 –2.6
2480...3700	inclined			+0.073			–
3700...3800			$\vartheta = 13^\circ.7$	+0.068	–	0	+3.3
3800...4150	Zenith angle decline	140×10.5	$\vartheta = 13^\circ.7...0^\circ$ $\Delta\vartheta = -0^\circ.4$	+0.23 +0.11	–1432	–1.25	+9.8 –9.8
4150...4680	vertical		0°	0	–	0	–

The theoretical analysis of the well design has shown that the axial force in the body of the column with increasing depth decreases piecewise linearly on straight sections (vertical and inclined), as well as on the curved ones along a circular arc. The latter is due to the small values of the zenith angles, which is consistent with the results of [3]. The same nature has the distribution of tensile stresses in the body of the pipes. At the same time, a discontinuous change in the stresses of two types was detected. The first type (on the marks of 1200 m and 3700 m) is caused by a change in the standard size of the casing pipes.

The second type of stress jumping is typical for the column curving intervals (with a constant radius of curvature according to the program) and is determined by the value of the bending moment created by the curvature. In addition, jumps of well wall reactions in the regions of the conjugation of its rectilinear and curved areas occur.

The jump-like nature of the change in the stresses and reactions of the walls is due to the fact that in the transition from rectilinear areas of the design well to those curved along a circular arc there is no geometric break of its axis, since the tangents coincide in the transitional section. However, the jump in the bending moment occurs, which is on the arc and is proportional to the curvature, but is absent on a straight line.

This is a consequence of the idealization of the project, in the first place, through the description of the distorted areas by the arc of the ideal circle. In a real well, the diameter of which is slightly larger than the diameter of the pipes, the edges of the column at the conjugated sites due to the elasticity of the pipes receive variable curvatures, which acquire values from R^{-1} on the arc section to 0 on a straight line and vice versa.

A positive well reaction indicates that the casing column rests on its lower wall; this is observed on inclined rectilinear and in the areas of the decline of the zenith angle (table 1). The negative reaction of

the walls shows that the column rests on the upper wall of the well due to the forces of elasticity of the initially rectilinear casing; this is manifested in the area of the zenith angle buildup. On the inclined sections, the reaction of the well coincides with the reaction of the inclined plane. On curved areas, the reaction of the walls varies, but given the small lengths of the arcs, its change can be considered linear. These results are consistent with the conclusions [3].

The numerical analysis program also worked out the program of the well number 170, given in the form of inclinometric table; the results of this are presented in figure 2 by lines 1. Patterns of the distribution of axial forces, the reactions of the well walls, bending moments, maximum stresses in the body of the column, obtained by numerical analysis and calculated by analytical formulas [3], qualitatively coincide completely.

The quantitative evaluation showed that the greatest difference between the numerical and theoretical calculation of axial forces in the project is observed near the conjugation of rectilinear and arc sections of the well. In the intersection between the vertical section and the arc with the zenith angle buildup it reaches 3.2%, in the intersection between the inclined and the arc with a downward angle it reaches 3.0%. On average, on straight and long arc sections, the difference is 1.5...2.5%.

The difference between the numerical and theoretical calculation of the reactions of the walls of the well project is found only in the arc sections (an average of 0.7...1.5%). The greatest difference is near the jump of the reaction value: 2.8% at the beginning of the section of zenith angle buildup and 2.1% at the beginning of the decline. On rectilinear sections (in particular, on inclined ones), the calculations of reactions give the same values.

The error of the developed numerical analysis method is due to the inaccuracy of numerical differentiation and integration and depends first of all on the choice of the value of the interval [6]. The difference between the numerical and theoretical calculations of the design maximum stresses in the body of the pipes is 0.01...0.03% along the entire column.

In addition, the developed program of numerical analysis worked out inclinometric table of data of field measurements of the actual well number 170; the results of this are presented in figure 2 by lines 2. This allowed to reveal the following features of the behavior of the casing in a real drilled borehole.

The graphs of the theoretical and actual axial forces practically coincide (fig. 2b). The difference between them on the vertical section increases from 2.2% to 3.3% in the cross section where the bending of the well and the zenith angle buildup begin. The greatest value of this difference lies in the lower part of the inclined area and in the transition from the inclined to the vertical one – to 4.6%. On other inclined and deviated areas the difference is 1...3%. However, these estimates of axial forces can not be attributed to the error of the numerical method (since different data have been processed – design and actually measured ones). First, they indicate a satisfactory coincidence in the whole of the design and drilled wells, as shown in figure 2a.

The actual deviation of the real well profile from the design one is shown by a graph of bending moments (fig. 2d), which can also be considered as a graph for changing the actual curvature of the well, since they are proportional according to (23). As you can see, the axis of an actual drilled well significantly deviates from the design profile (rectilinear or radius one). This is evidenced by the continuous change in bending moments by both magnitude and direction, which is caused by a change in the actual values of the local curvature of the well. This is due to the impact of a large number of technical, technological and geological factors on the drilling process.

Under these conditions, a casing column, trying to preserve its initially rectilinear form, at the expense of the forces of elasticity rests on opposite walls of a stochastically curved well, causing variables in magnitude and direction of reaction (fig. 2c). By comparing figures 2c and 2d, we can see that the magnitude and change of the local curvature of the well causes a proportional value and a change in the reaction of its wall. The reaction of the wall is also proportional to the bending rigidity of the casing. Accordingly, the internal bending moment and bending stress in the body of the pipe also change.

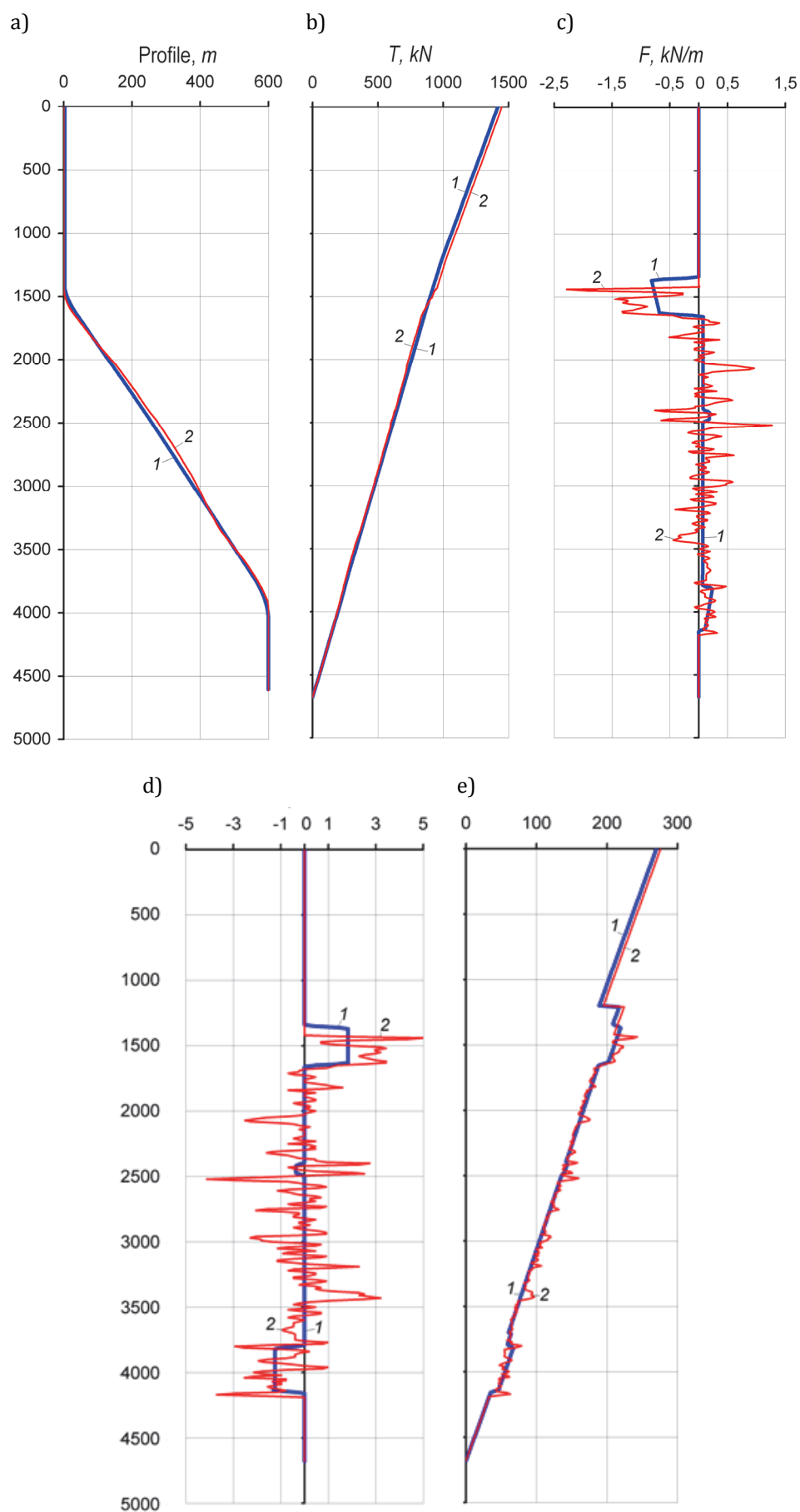


FIGURE 2. Wells profile (a), graphs of axial forces T (b), walls reactions F (c), bending moments M (d) and normal tensions σ (e) in column combined at depth intervals; where: 1 – according to the well project, 2 – according to inclinometric measurements

The largest jump in the values of the reaction of the actual well walls, the bending moment and the maximum stresses in the body of the casing is observed at a mark of 1440 m, where the actual deviation of the well and zenith angle buildup (as opposed to the design of 1350 m) begin. Along with this, the results of numerical analysis of an actual well made it possible to detect its areas with a significant increase in the curvature and the reaction of the wall. These are areas where the forced deviation of the well (zenith angle buildup and decline) occurred. In addition, in the areas of stabilization of the zenith angle, one can also find a local increase in the curvature and the reaction of the wall.

Numerical analysis of the stresses shows that for this well profile the tensile stress of the column is dominant (fig. 2e). Local stresses are of fluctuating nature and are related to the increase of local curvature of the well and bending moment in the column.

Applying results

The developed method of numerical analysis of the well allows detecting the areas with a significant local increase in the curvature, which indicates their obstructed passability. It allows one to accurately determine the depth intervals for increasing the well diameter. This must be done before lowering the casing string.

In addition, according to the results of the analysis, it is possible to determine the parameters of the stress-strain state of the casing, which can be used to predict its working capacity and operating life in the curved well.

Conclusions

The stress-strain state of the casing in the curved well can be determined by the non-uniform system of differential equations, which describes the bending of a long elastic rod under the action of distributed forces of its own weight, the reaction of supports and friction. Having the shape of the well with a known function of the zenith angle, we can find the solutions of the system in the form of functions of the distribution of axial forces and bending moments in the body of the column, as well as the reactions of the walls, which lead the column to the actual well profile.

Parameters of the stress-strain state of the casing in an actually drilled well can be determined by the developed methods of numerical integration of the data of inclinometric measurements of the well and the software of their numerical analysis. This allows us to identify areas of local increase in curvature and obstructed passability of the curved well.

References

- [1] Pesliak Yu.A.: *Calculation of stresses in columns of pipes of oil wells*. Nedra, Moscow 1973 (in Russian).
- [2] Vyslobitskyi P.A.: *Calculations of boundary states of pipe columns and pipelines*. Lotos, Kyiv 1997 (in Ukrainian).
- [3] Paliichuk I.I.: *The Interaction of the Casing String with the Walls of an Inclined, Curved and Horizontal Borehole Areas*. *Prospecting and Development of Oil and Gas Fields*, 1 (66), 2018, pp. 27-37 (in Ukrainian).
- [4] Frisch-Fay R.: *Flexible Bars*. Butterworths, London 1962.
- [5] Matveiev N.M.: *Methods of Integration of Ordinary Differential Equations*. Vysheishaia shkola, Minsk 1974 (in Russian).
- [6] Liashchenko M.Ya., Golovan M.S.: *Numerical Methods Tutorial*. Lybid, Kyiv 1996 (in Ukrainian).

Tatiana KUGAEVSKA

Vladimir SHULGIN

Poltava National Technical Yuri Kondratyuk University, Ukraine

PROCESSES OF MASS TRANSFER IN PERIOD LOADING CHAMBER OF CONCRETE PRODUCTS

Abstract: *Proposed investigate variety heat treatment of concrete and reinforced concrete products using only the heat released during cement hydration. The peculiarity of this variety consists in that the surface of products not hydro-insulated. Accordingly, in the thermal chamber than heat exchange processes the processes of mass transfer between the surface products and the air chamber. In the quantitative analysis of these processes is necessary to know number the initial factors, among them – the moisture content of the air chamber.*

The processes of heat and mass transfer between the surface of concrete and reinforced concrete products and air chambers begin already during loading them into the camera. During the loading of products is air combined with air workshop. Therefore for each case must quantify the impact of mass transfer processes on the initial moisture content of the air chamber.

Considered dependence that characterizes the process of evaporation of moisture from the surface of concrete products. Results of calculating the amount of moisture that evaporates from the surface of concrete paving slabs during selected period of time.

In further research is necessary to analyze the processes of heat and mass transfer in the chamber, where the heat treatment of concrete or reinforced concrete products (non-hydro-insulated) is using only the heat released during cement hydration.

Keywords: *concrete and ferroconcrete products, mass transfer processes, hydration of cement.*

Introduction

Implementation of thermal treatment of concrete and reinforced concrete products using only the heat released during cement hydration needs a number of experimental and computational studies [1-4].

Review of recent sources of research and publications

The interaction of cement with water heat released [2, 4-9]. In the patent [1] proposed to carry out heat treatment of concrete and reinforced concrete products using only the heat released during cement hydration. In the patent notes that the products before loading into the heat-insulating chamber covered with polyethylene film (or other hydro-insulation material) to store in products moisture needed for hydration of cement. However, it is necessary to investigate the way heat treatment of concrete and reinforced concrete products using only the heat released by the interaction of cement with water, in which the surface of products not hydro-insulated. In this case, will be mass transfer between the surface of products and the environment of the camera.

In the book [10] shows the processes of heat and mass transfer during evaporation and condensation of liquid. In the book [11] show the processes of heat and mass transfer in steam treatment concrete and reinforced concrete products using steam.

Determination unsolved before parts problems

The processes of heat and mass transfer between the surface of concrete and reinforced concrete products and air chambers begin already during loading them into the camera. It is advisable to conduct a quantitative analysis of these processes.

Formulation of the problem

Purpose of the article – the analysis of mass transfer processes between the surface of concrete products and air thermal chamber when loading them into the camera.

The basic material and results

The processes of mass transfer between the surface of concrete and ferroconcrete products and air thermal chamber during loading them into the camera. These processes are interconnected with the processes of heat transfer in the chamber.

There are three main cases the direction of heat flow and flow of water vapor during this period. First case:

- temperature of concrete and ferroconcrete products t_c lower than the air temperature workshop t_w and temperature t_c constructions enclosing chamber for thermal treatment of concrete products;
- temperature of concrete products t_c higher than the temperature «dew point» t_{PDP} .

The direction of heat flow in the chamber at this time is reflected in figure 1. In this case, the partial pressure of water vapor the air chamber or lower or higher than the partial pressure of water vapor near the surface of the concrete mix. Directions mass flow depends on the ratio between the partial pressure.

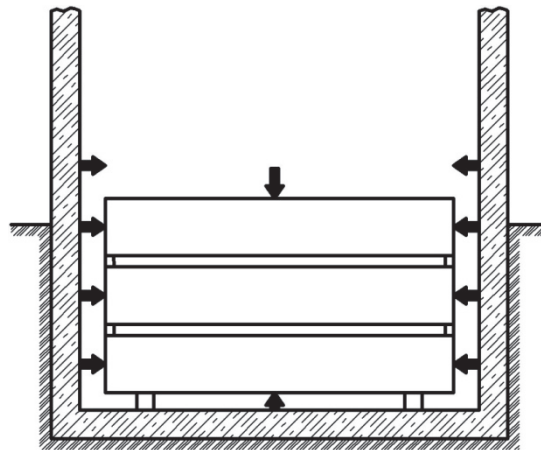


FIGURE 1. Scheme of heat flow in the chamber during loading of products (the first case)

The second case:

- temperature of concrete and reinforced concrete products t_c higher than the air temperature workshop t_w and temperature t_c constructions enclosing chamber for thermal treatment of concrete products;
- air temperature chamber is higher than the temperature "dew point" t_{DP} .

The direction of heat flow in the chamber at this time is reflected in figure 2. In this case, the partial pressure of water vapor the air chamber lower than the partial pressure of water vapor near the

surface of the concrete mix. Accordingly, will occur evaporation of moisture from the surface of products.

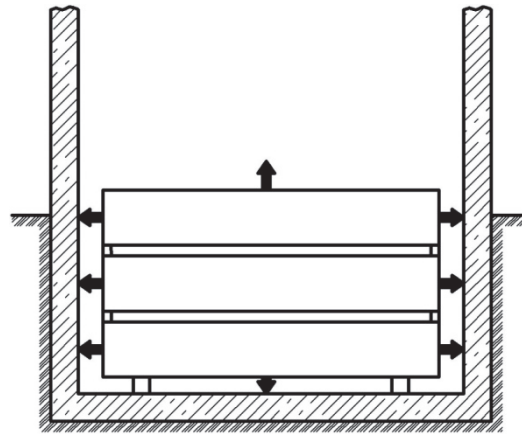


FIGURE 2. Scheme of heat flow in the chamber during loading of products (second case)

The third case: $t_c = t_w > t_{DP}$

Consider the cases when the partial pressure of water vapor near the surface formed concrete products higher than the partial pressure of water vapor in the air chamber. The surface of the concrete products during their formation and stay in the chamber while loading – moisture. So take approximately that evaporation of moisture from the surface of the product in this period is similar to evaporation of moisture from the surface of water.

The amount of moisture W , that evaporates from the surface of the product per unit of time, kg/s, determined by the formulas given in particular the book [10]:

$$W = \beta' \cdot (P_{SC} - P_{AIR}) \cdot (101325 / P_B) \cdot F \quad (1)$$

$$W = \beta \cdot (C_{SC} - C_{AIR}) \cdot (101325 / P_B) \cdot F \quad (2)$$

the amount of moisture $W_{\Delta\tau}$, that evaporates from the surface of the product for a certain period of time $\Delta\tau$, kg, calculated by the formulas:

$$W_{\Delta\tau} = \beta' \cdot (P_{SC} - P_{AIR}) \cdot (101325 / P_B) \cdot F \cdot \Delta\tau \quad (3)$$

$$W_{\Delta\tau} = \beta \cdot (C_{SC} - C_{AIR}) \cdot (101325 / P_B) \cdot F \cdot \Delta\tau \quad (4)$$

where:

β' – mass transfer coefficient (mass returns), referred to the difference of partial pressures ($P_{SC} - P_{AIR}$), $\text{kg}/(\text{m}^2 \cdot \text{s} \cdot \text{P})$;

β – mass transfer coefficient (mass returns), referred to the difference of water vapor concentration ($C_{SC} - C_{AIR}$), m/s ;

P_{SC} – the partial pressure of water vapor near the surface of the concrete product, P;

P_{AIR} – the partial pressure of water vapor in the air chamber, P;

C_{SC} – the concentration of water vapor near the surface of the concrete product, kg/m^3 ;

C_{AIR} – the concentration of water vapor in the air chamber, kg/m^3 ;

P_B – barometric pressure, P;

F – area open surface of concrete products, m^2 .

The concentration of water vapor in the air chamber is calculated by dependence

$$c_{AIR} = \frac{P_{AIR} / 133.322}{3.463(273 + t_{AIR})} \quad (5)$$

the concentration of water vapor in the air near the surface of the product is calculated by dependence

$$c_{SC} = \frac{P_{SC} / 133.322}{3.463(273 + t_{SC})} \quad (6)$$

where:

t_{AIR} – air temperature chamber, °C;

t_{SC} – the surface temperature of the concrete product, °C.

Mass transfer coefficient β , m/s, is equal to

$$\beta = Nu' \frac{D}{L} \quad (7)$$

where:

Nu' – diffusion Nusselt number;

D – the diffusion coefficient, m²/s;

L – the determining size, m.

For water vapor the diffusion coefficient, m²/s, calculated by the formula given the book [10]

$$D = 0.0754 \cdot \left(\frac{T}{273} \right)^{1.89} \cdot \frac{101325}{P_B} \quad [\text{m}^2/\text{h}] \quad (8)$$

$$D = 0.0754 \cdot \left(\frac{T}{273} \right)^{1.89} \cdot \frac{101325}{P_B} \cdot \frac{1}{3600} \quad [\text{m}^2/\text{s}] \quad (9)$$

$$T = t + 273 \quad (10)$$

$$t = 0.5 \cdot (t_{AIR} + t_{SC}) \quad (11)$$

where:

T – absolute average air temperature is, K;

t – average air temperature is, °C.

Diffusion Nusselt number can be determined by the formula given in the book [10]:

$$Nu' = 0.66 \cdot (Ar \cdot Pr')^{0.26} \quad (12)$$

(at $Ar \cdot Pr' = 3 \cdot 10^6 - 2 \cdot 10^8$)

where:

Ar – Archimedes criterion;

Pr' – diffusion Prandtl number.

Diffusion Prandtl number is equal to

$$Pr' = \frac{\nu}{D} \quad (13)$$

where:

Pr' – diffusion Prandtl number;

ν – kinematic coefficient of viscosity of air at an average temperature of air t , m²/s.

Archimedes criterion is equal to

$$Ar = \frac{L^3 g}{\nu^2} \cdot \frac{\Delta\rho}{\rho} \quad (14)$$

$$L = \sqrt{F} \quad (15)$$

where:

L – the determining size, m;

F – area open surface of concrete products, m²;

g – acceleration of gravity, m/s²;

$\Delta\rho$ – air density difference, kg/m³.

The density of the air chamber, kg/m³, calculated by dependence

$$\rho_{AIR} = 1.293 \cdot \frac{273}{T_{AIR}} \cdot \left(\frac{101325}{P_B} - 0.378 \cdot \frac{P_{AIR}}{101325} \right) \quad (16)$$

air density near the surface of the wet concrete mixture, kg/m³, calculated by dependence

$$\rho_{SC} = 1.293 \cdot \frac{273}{T_{SC}} \cdot \left(\frac{101325}{P_B} - 0.378 \cdot \frac{P_{SC}}{101325} \right) \quad (17)$$

where:

P_{AIR} – the partial pressure of water vapor in the air equipment, P;

P_{SC} – the partial pressure of water vapor near the surface of the concrete product, P.

In the table 1 shows examples of calculating the amount of moisture that evaporates from the surface of concrete paving slabs in the first 15 minutes she was in the chamber

TABLE 1. Number of moisture that evaporates from the surface of concrete paving slabs

$t_{AIR}, ^\circ\text{C}$	$\varphi_{AIR}, \%$	$T_{SC}, ^\circ\text{C}$	$W, \text{kg/s}$	$W_{\Delta\tau}, \text{kg}$	$\Delta\tau, \text{h (s)}$	F, m^2
20	65	18	$4.52 \cdot 10^{-6}$	0.0041	0.25 (900)	0.5
20	65	20	$5.91 \cdot 10^{-6}$	0.0053	0.25 (900)	0.5
20	55	20	$8.12 \cdot 10^{-6}$	0.0073	0.25 (900)	0.5
20	65	22	$1.12 \cdot 10^{-5}$	0.0101	0.25 (900)	0.5
25	65	25	$8.67 \cdot 10^{-6}$	0.0078	0.25 (900)	0.5
25	55	25	$1.19 \cdot 10^{-5}$	0.0107	0.25 (900)	0.5

Evaporated from concrete or reinforced concrete products water vapor increases the moisture content of the air chamber. During loading products air chamber combined with air workshop. Therefore for each case must quantify influence of processes mass transfer on moisture content of the air chamber. This moisture content is one of the primary parameters in the analysis of heat and mass transfer in the chamber, where the acceleration of hardening concrete products (non-hydro-insulated) occurs without the use of coolant.

Conclusions

Considered the processes of mass transfer during the loading of concrete or reinforced concrete products in the thermal camera.

In further research is necessary to analyze the processes of heat and mass transfer in the chamber, where the heat treatment of concrete or reinforced concrete products (non-hydro-insulated) is using only the heat released during cement hydration.

References

- [1] Pat. № 90487. Ukraine. MPC C04B 40/02 (2006.01). The method of heat treatment of concrete and concrete products / T.S. Kugaevska, V.V. Shulgin; the applicant and owner of Poltava National Technical Yuri Kondratyuk University.; appl. 13.01. 2014; publ. 26.05.2014, bul. № 10.
- [2] Kugaevskaya T.S.: *Development of prediction method of concrete products temperature changes under their curing*. T.S. Kugaevskaya, V.V. Shulgin, Conference reports materials «Problems of energy saving and nature use 2013», Budapest 2014, pp. 46-52.
- [3] Kugaevska T.S.: *Definitions consumption of heat on heating designs chambers for thermal treatment concrete products*. T.S. Kugaevska, V.V. Shulgin, Collection of scientific articles «Energy, energy saving and rational nature use», Kazimierz Pulaski University of Technology and Humanities in Radom, № 1 (4) Radom 2015, Poland 2015, pp. 42-45.
- [4] Kugaevska T.: *Development of methodology forecasting of intensity solidification concrete products in the alternative methods of heat treatment*, Energy, energy saving and rational nature use, Oradea University Press, 2015, pp. 4-52.
- [5] Volzhenskij A.V.: *The mineral binders substances*. A.V. Volzhenskij. M: Strojizdat 1986, 464 p.
- [6] Mchedlov-Petrosjan O.P.: *Heat release of hardening binding substance and concretes*. O.P. Mchedlov-Petrosjan, A.V. Usherov-Marshak, A.M. Urzhenko, M: Strojizdat, 1984, 224 p.
- [7] Lotov V.A.: *Heat generation in the cement-water upon hydration and hardening*. V.A. Lotov, E.A. Sudarev, J.A. Ivanov. Stroitelnye materialy, 2011, No. 11, pp. 35-37.
- [8] *Temperature monitoring hardening cement systems*. A.V. Kabus', N.N. Isaenko, E.A. Moroz. E.V. Ivashhenko, E.B. Voropaeva. Naukovij visnik budivnictva. Issue 65, KNUCA, Kharkiv 2011, pp. 256-263.
- [9] Livsha R.J.: *Evaluation exotherm at an early stage hardening cement-concrete coatings* [Electronic resource]. R.J. Livsha, L.O. Karasova. Access mode: <http://ena.lp.edu.ua:8080/bitstream/ntb/7655/1/25.pdf>.
- [10] Nesterenko A.V.: *Basics of thermodynamic calculations of ventilation and air conditioning*. A.V. Nesterenko. M: Vyssh. shkola, 1971, 460 p.
- [11] Marjamov N.B.: *Heat treatment of products in the factories of precast reinforced concrete*. N.B. Marjamov, M: Publ. liter. for the construction, 1970, 272 p.

Anatoliy M. PAVLENKO

Kielce University of Technology, Poland

Andrii CHEILYTKO

Zaporizhzhya State Engineering Academy, Ukraine

INVESTIGATION OF THE PROCESS OF PORE FORMATION BASED MATERIALS HYDROSILICATES

Abstract: *Research porosity thermal insulation of refractory materials is the important task of power engineering, because the thermal conductivity of porous materials depends on the shape and especially location of pore.*

Analytical review of existing technologies shows that research in this area focused on the study of a process separately and generalized theories is not sufficient to clear analysis and model building process heat mass transfer of alumina porous material. Experimental and generalization of the characteristics of heat and mass transfer in porous materials that swelling is actual scientific problem.

In this paper analyzes the different composition of aluminous minerals, aluminum effect of additives on the formation of pores, as well as the influence of various impurities on the thermal conductivity of the material. The effect of temperature on the thermal conductivity of porous materials.

Keywords: *thermal conductivity, porosity, swelling, heat insulation.*

Introduction

Argil – widespread rock formation unstable composition and physical properties. Pure argil – clay without any impurities, is rock consisting of small dispersed particles of a certain chemical composition (which includes the base hydroaluminosilicates). Argil has a property to become plastic when saturated with moisture and maintain its form during drying. Argil is a silicate which includes alumina, silica, bound water, sand, lime carbonate, etc. The density of the argil is usually in the natural humidity of 25% the total of 1500÷1600 kg/m³. From argil made such important heat insulation materials such as brick and ceramsite. The properties of these materials depend on the chemical composition of particulate matter fraction included in its composition [1].

Many experimental data indicate the presence of relationship between the porosity of the material and its thermophysical properties [2]. Influence of porosity on the thermal conductivity of the material can be considered following the example of experimental data [3]. The values of thermal conductivity of iron (58.19 W/(m·K)) and a rock formation (3.26 W/(m·K)) are different almost 18 times, but the filling of iron balls and balls a rock formation of the same porosity of 62.5% has nearly the same coefficient of thermal conductivity (0.0403 W/(m·K) and 0.0402 W/(m·K) respectively. However, the way of forming the porous structure has not yet been investigated, and accurate relationship between the porosity and the physical properties of the material not found.

In [2] analyzed the basics the formation of pores, but there is no end link of the form of the porous structure of a material with its thermophysical characteristics. It is also still not clear how necessary to evaluate the porous structure. Most authors studying porous materials are evaluated only quantitative indicator - porosity. The question of the adequacy of the criterion has not yet been raised.

The main part of research

To conduct a series of experiments on the swelling of hydrosilicates chosen argil different places of birth, with a different chemical composition. For the heat treatment used muffle furnace with thermocouples HC-0.1.

The used argil was classified visually ductility and the results are summarized in table 1. We used the following scale:

- 0 – dry powder,
- 1 – not plastic, at low load is divided into small pieces,
- 2 – not plastic, at low load is divided into large pieces,
- 3 – not plastic, destroyed only under heavy load,
- 4 – plastic.

TABLE 1. *The characteristics of the argil*

No. sample	Colour	The plasticity	The presence of impurities
1	yellow	3	small
2	dark grey	2	medium
3	mustard	4	small
4	mustard	3	medium
5	gray	3	large
6	gray	3	large
7	gray	3	large
8	gray	3	large
9	mustard	4	medium
10	dark grey	3	medium
11	white argil	0	not available

These samples were filled to the maximum humidity. A portion of each sample was dried and rapid indirect method (10 minutes of drying time, oven temperature 130°C) was determined by the humidity of the samples (table 2). The color of the resulting material can be seen on the progress of the main reactions. So red-brown color of the material will indicate oxidation processes, dark gray color of the recovery process.

The dried samples had the following characteristics:

- part of the sample No. 1 - color - yellow mustard, appeared pores fragile;
- part of the sample No. 2 - color - has not changed, visible small pores and cracks, more robust;
- part of the sample No. 3 - color - yellow mustard, you can see a few small pores;
- part of the sample No. 4 - color - yellow mustard, clearly visible pores and layers, brittle;
- part of the sample No. 5 - color - has not changed, visible layers;
- part of the sample No. 6 - color - has not changed, there is clearly split into two main layer;
- part of the sample No. 7 - color - has not changed, there were pores and cracks;
- part of the sample No. 8 - color - mustard-gray, appeared pores and layers;
- part of the sample No. 9 - color - yellow mustard, were pores and cracks;

- part of the sample No. 10 - color - has not changed, visible small pores and cracks;
- part of the sample No. 11 - color - has not changed, clearly visible spherical pores, not available layers and cracks, brittle.

TABLE 2. Determine the moisture content of the initial mixture

No. sample	Weight before drying	Weight after drying	Weight of absorbed water	Humidity W,%
1	12.9	12	0.9	6.9767
2	17.7	16.9	0.8	4.5198
3	20.2	11.4	8.8	43.564
4	17.1	14.3	2.8	16.374
5	15	10.4	4.6	30.667
6	13.7	9.5	4.2	30.657
7	20.8	14.6	6.2	29.808
8	17.9	13.1	4.8	26.816
9	19.5	13.9	5.6	28.718
10	10.4	7.3	3.1	29.808
11	10.4	6.5	3.9	37.5

From the experiment it is seen that the evaporation of moisture causes the formation of pores inside the argil. It has highest porosity pure argil, wherein the pores are spherical in nature. The presence of impurities reduces the porosity of the material, as it increases the viscosity of argil. It should be noted that the impurities will also affect the shape of the pores. The pores are becoming stretched perpendicular to the lines of diffusion of moisture, the material is separated into individual layers. A large number of impurities leading to formation of cracks. This is due to the uneven distribution of impurities in volume, thus creating different tensions within the material in pore formation. Also impurities increase the final strength of the material.

To determine the effect of triatomic gases swelling process samples available swelling at 750°C for 8 minutes. This temperature is enough for allocation the gases, but it is lower than the melting temperature of the argil. After heat treatment, all samples were observed following changes: pore – are bigger than in the previous experiment, but is not spherical; sometimes there is a great time to within the material; the material becomes more durable, that is connected with chemical reactions; there are more distinct crack; material from pure argil is still fragile, but more irregular pores, and various size.

Investigation of the effect of additives on aluminum swelling of argil

Presumably aluminum must enter into relationship with hydroxides and water, thereby forming a new chemical compound. The increase in aluminum oxide will change the structure and physical properties of argil. The samples were saturated with moisture, and they added different amounts of aluminum. The heat treatment temperature is equal to 750°C, time 8 minutes. The experimental data are listed in the tables 3 and 4. Moisture and devolatilization gases was determined by the indirect method, accelerated.

Results of the experiment are summarized in figure 1 grid is applied to calculate the porosity. Graduation 1 mm.

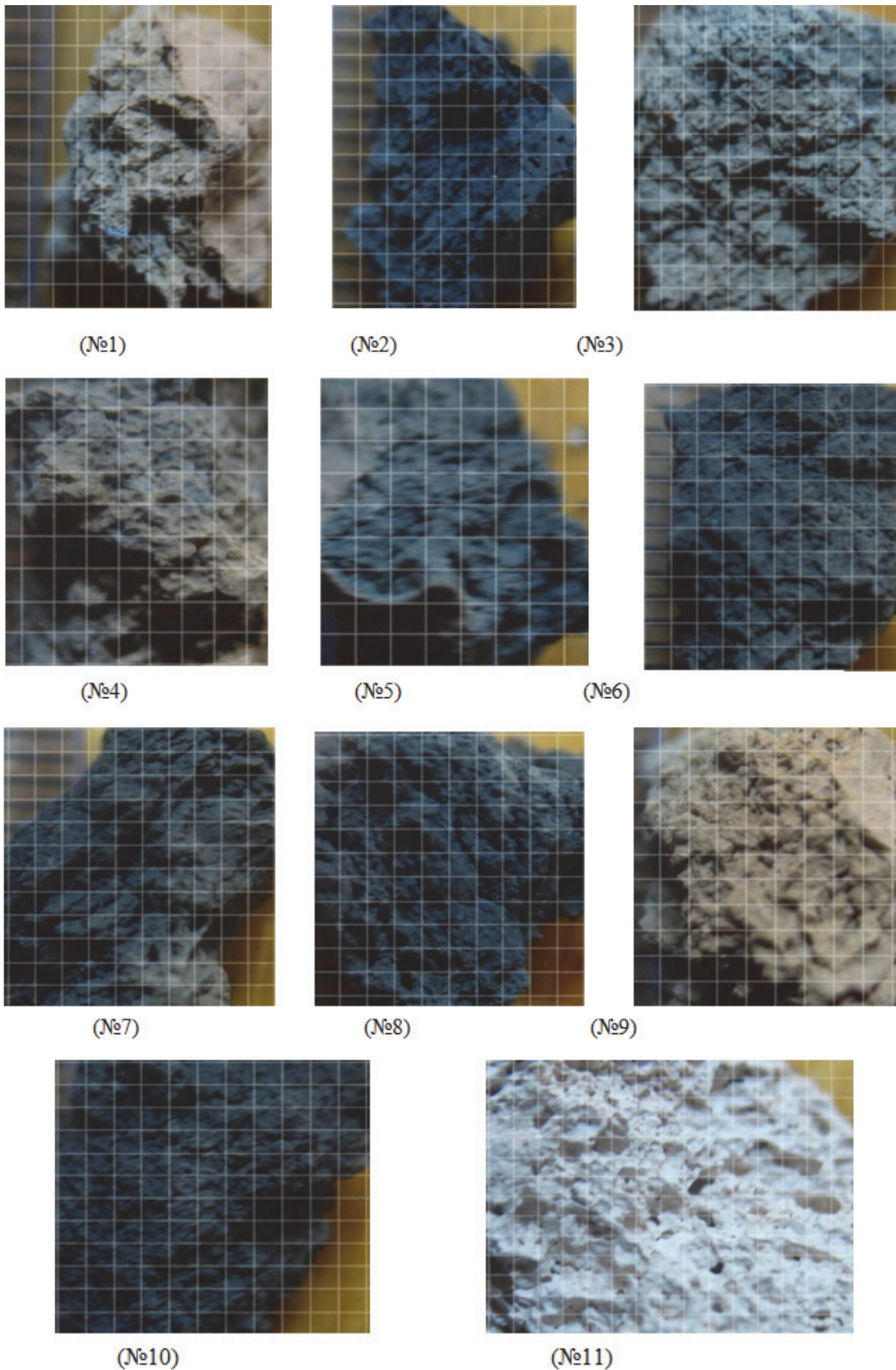


FIGURE 1. Expanded samples of argil with the addition of aluminum

Expanded samples had the following characteristics:

- part of the sample No. 1 - a color in the middle of - sand, crust color - yellow with orange flavor, closer to the center there is separation of layers (elongated wedge-shaped pores), harder than without the addition of aluminum;

- part of the sample No. 2 - color - black, visible small pores and cracks, pores are quite a bit larger than the pore formation of moisture, more robust; aluminum particles are seen, which did not react with the silica;
- part of the sample No. 3 - color - sandy, more clearly visible pores, there are small cracks, well traced the inner layer with low porosity;
- part of the sample No. 4 - color - gradient from gray to yellow-orange, clearly visible pores of different sizes, more durable;
- part of the sample No. 5 - the color of the outside - orange hue color of inside - gray, fine porosity, and visible separation into layers, in some places there are large pores;
- part of the sample No. 6 - color - black, visible small pores and cracks, a strong, visible aluminum particles that do not react with the silica;
- part of the sample No. 7 - color outside - dark yellow inside color - black, clearly visible separation into layers, the surface layer of small spherical pores visible, the aluminum particles are visible which are not reacted with the silica;
- part of the sample No. 8 - color outside - gray inside color - black, clearly visible separation into layers, the surface layer of small spherical pores visible, the aluminum particles are visible which are not reacted with the silica;
- part of the sample No. 9 - color - yellow-orange with a small plot of gray inside the sample, clearly visible pores and small cracks;
- part of the sample No. 10 - color outside - gray visible small spherical pores, but the pores predominate vermiculite, aluminum particles are seen, which did not react with the silica;
- part of the sample No. 11 - appeared in some places a shade gray in color, the pores are larger, there was strongly pronounced channel porosity. Channel porosity occurred during draining different pores.

After the experiments it can be concluded that aluminum in argil with a large amount of impurities and a high content of humus practically does not react and no effect on swelling of. In the argil with a small amount of impurities – small additions of aluminum is slightly increased strength properties and slightly increases the porosity. In pure argil small additions of aluminum greatly increase pore formation. In general, all the samples of aluminum additives do not affect the shape of the pores. In samples where aluminum is not reacted, it can be seen near the germ pores aluminum particles. In pure argil all also absent vermiculite pores.

TABLE 3. *Moisture and the amount of volatile gases in the test samples*

No. sample	Humidity W, %	Weight of the pure sample before drying, g	Al weight before drying, g	Al weight after drying, g	Weight Al, g	Al, %	Vro ₂ +W, %	Vro ₂ , %
1	6.9767	6.1	6.3	4.1	0.2	3.1746	34.921	27.944
2	4.5198	3.5	3.7	2.5	0.2	5.4054	32.432	27.913
3	43.564	5.1	5.2	2.7	0.1	1.9231	48.077	4.5126
4	16.374	6.3	6.5	4.6	0.2	3.0769	29.231	12.857
5	30.667	7.3	7.4	4.7	0.1	1.3514	36.486	5.8198
6	30.657	6.8	6.9	4.5	0.1	1.4493	34.783	4.1257
7	29.808	9.8	9.9	6.6	0.1	1.0101	33.333	3.5256
8	26.816	7.6	7.7	5	0.1	1.2987	35.065	8.2493
9	28.718	5.6	5.8	3.6	0.2	3.4483	37.931	9.2131
10	29.808	6.7	6.8	4.3	0.1	1.4706	36.765	6.957
11	37.5	7	7.2	3.4	0.2	2.7778	52.778	15.278

TABLE 4. The porosity and frost resistance of test samples

No. sample	The number of pores per 20 mm ²						Limit the number of cycles of wetting - drying	Limit the number of cycles of freeze defrosting
	vermiculite			spherical				
	<1 mm	1-3 mm	>3 mm	<1 mm	1-3 mm	>3 mm		
1	7	1	0	11	0	1	15	17
2	6	1	1	0	0	0	7	9
3	10	1	1	10	1	0	10	11
4	4	0	0	25	3	0	8	9
5	5	1	0	7	1	0	15	13
6	12	1	1	21	0	0	9	8
7	5	4	1	1	0	0	15	14
8	13	3	1	6	0	0	12	13
9	6	1	0	8	2	0	12	13
10	4	2	0	7	0	0	11	11
11	0	0	0	28	4	1	5	3

Determination of the effect of porosity on thermal conductivity

Previously described numerous analytical and empirical studies of the effect of porosity and bulk density on the thermal conductivity of the final material or layer. It was shown that all dependencies have their uses and are not suitable for general cases. Some dependencies absolutely not suitable for calculating the thermal conductivity of porous material. Therefore, experiments were conducted to determine the thermal conductivity of different porous materials. We investigated samples of expanded argil (sample number 2, 3, 4), the sample $3\text{CaO} \cdot \text{Al}_2\text{O}_3 \cdot 6\text{H}_2\text{O}$ (sample No. 5) and pressed gypsum powder (sample No. 1). Samples of expanded argil differed only by the temperature of heat treatment. The temperature of the heat treatment of the sample No. 2 was 800°C, sample No. 3 – 650°C, sample No. 4 – 750°C. Measurements of thermal conductivity were performed on IT-λ-400. This measuring instrument is designed to study the temperature dependence of the thermal conductivity of solid, machined materials in the heating mode, a monotone, which allows one to get the experiment right temperature dependence of the studied parameters and provide high performance. The theoretical basis of the method described in [4].

Working calculation formulas for the thermal resistance of the sample and its thermal conductivity are given below [5].

The thermal resistance of the sample was the following formula

$$P_0 = \frac{\nu_0 \cdot S \cdot (1 + \sigma_c)}{\nu_T \cdot K_T} - P_k$$

where:

K_T – coefficient of proportionality is characterized by the effective thermal conductivity of the plate (constant value for the device is in the calibration), W/K,

P_k – thermal contact resistance (constant value for the device),

σ_c – the amendment taking into account the heat capacity of the sample, the contribution does not exceed 10%,

ν_0 – temperature difference across the sample, K,

ν_T – temperature difference on the plate, K.

The amendment takes into account the heat capacity of the sample was determined by the following formula [6]

$$\sigma_c = \frac{C_0}{C_0 + 2C_r}$$

where:

C_0 – the total heat capacity of the sample, $C_0 = c_0(t) \cdot m_0$;

C_r – the total heat capacity of the rod, $C_r = c_c(t) \cdot m_r$;

c_0 – the approximate value of the mass specific heat of the sample, J/(kg·K);

c_c – the value of the mass the specific heat capacity of copper, J/(kg·K);

m_0 – sample weight, kg;

m_r – weight of the rod, kg.

This formula differs from the formula proposed by [5]. Its choices are substantiated by the fact that calibration ratio is calculated before it under this formula.

The thermal conductivity of the sample is determined by the following formula

$$\lambda = \frac{h}{P_0}$$

where h is sample height, m.

The calculated values of the thermal conductivity of the sample were attributed to the average temperature of the sample, which is determined by the formula

$$\bar{t} = t_c + 0.5 \cdot A_t \cdot n_0$$

where:

\bar{t} – the average temperature of the sample, °C;

t_c – the temperature at which the measurements, °C;

A_t – the sensitivity of the thermocouple CA, K/mV;

n_0 – temperature difference across the sample, mV.

The results of experiments and calculations were analyzed. With an increase in temperature from °C to 275°C the thermal conductivity of the porous material is increased. Moreover, the thermal conductivity pure Al_2O_3 when the temperature rises (within the specified range) should decrease [7]. This confirms the possibility of regulating thermal conductivity by increasing the content of Al_2O_3 . But based on previous experiments, it can be argued that the increase in content Al_2O_3 into alumina will be justified only when a minimum of impurities.

For all of the samples characteristic that all of the temperature dependence of the thermal conductivity of most accurately describes the logarithmic dependence.

Figure 2 shows the dependence of the thermal conductivity of five samples of the temperature. From this graph it can be concluded that the behavior of the thermal conductivity of all the samples of the same, but the dependence of aerated concrete has a gentle nature, i.e. It is minimally dependent on the temperature.

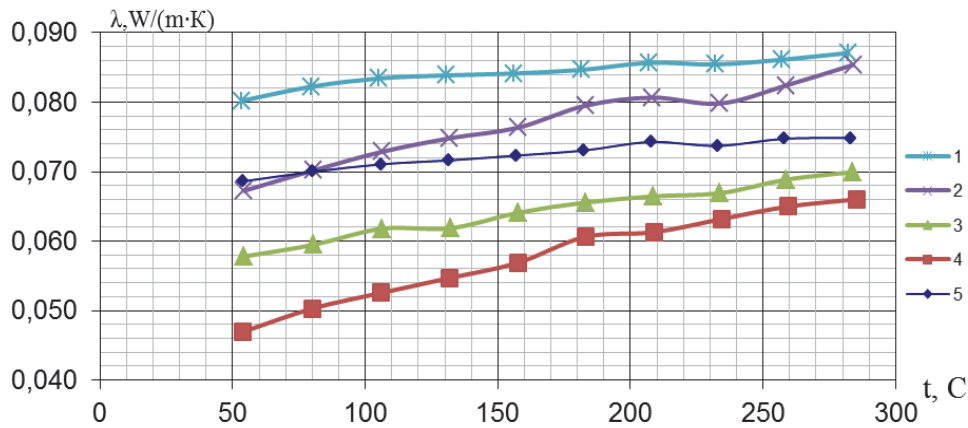


FIGURE 2. Dependence of thermal conductivity of samples on temperature

Dependence of the temperature swelling argil on the thermal conductivity is ambiguous.

The minimum thermal conductivity was achieved at 750°C. Moreover during the heat treatment of 650°C slightly higher than the thermal conductivity of the material, and at 800°C – substantially higher than twice. This is due to the uniformity of the pore distribution and the same size during the heat treatment of 750°C. Thus, when the heat treatment of 650°C – less uniform pores and smaller in size (sample less porous). At 800°C – a considerable increase in for some time, but disappear smaller pores and the total porosity of the material at greater than 750°C heat treatment, but the porosity is non-uniform. Also at 750°C and 800°C will be leakage of different chemical reactions that also significantly affected the results.

It can be concluded that the uniformity of the porosity has a significant effect on the thermal conductivity of porous building materials.

Conclusions

The presence of impurities in the intumescent of aluminous materials reduces the of the final porosity material. The pores are becoming stretched perpendicular to the lines of diffusion of moisture, the material is separated into individual layers. A large number of impurities leading to formation of cracks.

The amount of aluminum in the alumina has different effects on the process of swelling. The alumina with a large amount of impurities – aluminum practically does not react and do not affect the swelling. In the argil with a small amount of impurities – small additions of aluminum are slightly increased strength properties and slightly increase the porosity. In pure argil small additions of aluminum greatly increase pore formation. In general, all the samples of aluminum additives do not affect the shape of the pores.

Small content of Al_2O_3 mixture increases the duration blistering, and also increases the viscosity of the mixture. The iron content in the intumescent mixture should be kept to a minimum.

Dependence of the temperature swelling argil in the final thermal conductivity of the material is nonlinear.

The uniformity of porosity has a significant effect on the thermal conductivity of porous building materials.

References

- [1] Cheylitko A.O.: *Experimental studies thermophysical properties of the porous particulate material depending on different heat treatment conditions*. Eastern-European Journal of Enterprise Technologies. No. 5/6(41), 2009, pp. 4-7.

- [2] Cheylitko A.A.: *Study of vesiculation in intumescent material*. Technology audit and production reserves, 5/4 (13), 2013, pp. 38-40. Available at: <http://journals.uran.ua/tarp/article/view/18251/16063>.
- [3] Chudnovskij A.F.: *Teplofizicheskie karakteristiki dispersnyh materialov*. Gosudarstvennoe izdatel'stvo fiziko-matematicheskoy literatury, Moscow 1962, 456.
- [4] Shatunov E.S.: *Teplofizicheskie izmerenija v monotonnom rezhime* (Thermophysical measurements in a monotone mode). "Energija", 1972.
- [5] Denisova E.I., Shak A.V.: *Izmerenie teploprovodnosti na izmeritele IT-λ-400 Uchebnoe elektronnoe tekstovoe izdanie*. SEI HPE USTU, Ekaterinburg 2005.
- [6] Zhmetko D.M., Lemish P.V.: *Fizichni metodi doslidzhennja*. Praktikum dlja studentiv fizichnogo fakultetu.: ZNU, Zaporizhzhya 2008, pp. 77.
- [7] Gurtov V.A., Osaulenko R.N.: *Fizika tverdogo tela dlja inzhenerov*. Moscow 2007.

Hanna KOSHLAK

Ivano-Frankivsk National Technical University of Oil and Gas, Ukraine

THE THERMOPHYSICAL PECULIARITIES HEAT AND MASS TRANSFER INOCULATORS IN MELTS METALS

Abstract: The article presents the results of research of thermophysical peculiarities obtaining volumetric amorphous structures in metals and alloys. This technology differs mainly the realization internal heat removal by means of local heat sink (inoculator). A mathematical model of melting inoculator in melts for optimizing the process of obtaining massive amorphous structures, which allows to reduce time of experimental research and material resources to create massive amorphous structures. Mathematical modeling of processes heat and mass transfer inoculator in melts allows you to identify peculiarities of the technological process, and establish influence inoculator on the degree of amorphization melt. The results provide an effective assessment of the intensity of heat transfer during the casting process, which makes it possible to estimate and predict the ability of alloys to the amorphization of the structure.

Keywords: heat and mass transfer, amorphous structure, inoculator, thermal conductivity, mathematical model, cooling, melting

The physical statement of the problem

Consider the process of melting solid inoculator having a melting point t_L^T , completely immersed in molten metal with a given temperature t_p . In reality, the initial temperature inoculator t_0 always less temperature of solidification metal t_S^p and therefore, initially formed on its surface shell of solid metal. Further progress depends on the melting of the relationship between temperature values t_L^T , t_S^p , t_p [1]. In I inoculator period when immersed in the molten metal at its surface formed shell of solid metal. The heat coming from the melt by convection and solidification of metal on the surface, is spent on heating and melting inoculator shell melt. End of period determined by moment of complete melting of the shell. In the II period the solid inoculator heated to the melting point t_L^T and direct contact with the liquid alloy. In III period inoculator begins to melt and liquid phase body dissolved in the melt.

Mathematical model

On the surface inoculator the formation of solid metal shell with further melting of the shell. This period is described melting heat conduction equations for two-layer body, which includes the equation for the material body ($0 \leq r < R_i$) and for shell melt ($R_i \leq r < Z_M$) at $\tau > \tau_1 + \tau_2$:

$$\begin{cases} c_i(t)\rho_i(t)\frac{\partial t_i(r,\tau)}{\partial \tau} = \frac{1}{r}\frac{\partial}{\partial r}\left[r\lambda_i(t)\frac{\partial t_i(r,\tau)}{\partial r}\right], 0 \leq r < R_i \\ c_M(t)\rho_M(t)\frac{\partial t_M(r,\tau)}{\partial \tau} = \frac{1}{r}\frac{\partial}{\partial r}\left[r\lambda_M(t)\frac{\partial t_M(r,\tau)}{\partial r}\right], R_i \leq r < Z_M \end{cases} \quad (1)$$

Boundary conditions at $\tau > \tau_1 + \tau_2$:

on the axis of symmetry of the body ($r = 0$) given the symmetry condition [1]:

$$\frac{\partial t_i(0, \tau)}{\partial r} = 0 \quad (2)$$

at the interface between the material inoculator and the shell melt ($r = R_k$) given boundary conditions IV:

$$\lambda_i(t) \frac{\partial t_i(R_i, \tau)}{\partial r} = \lambda_m(t) \frac{\partial t_m(R_M, \tau)}{\partial r}, \quad t_i(R_i, \tau) = t_m(R_i, \tau) \quad ??? \quad (3)$$

of heat exchange condition on the boundary of frozen shell melt – melt ($r = Z_m$):

$$-\rho_m(t) Q_m \frac{dZ_m(\tau)}{d\tau} = \alpha_m (t_p(\tau) - t_v) - \lambda_m(t) \frac{\partial t_m(Z_m(\tau), \tau)}{\partial r} \quad (4)$$

$$t(z(\tau), \tau) = t_L, \quad 0 \leq z(\tau) \leq z_0, \quad \tau > \tau_2, \quad Z_m(\tau) > R_i, \quad \tau > \tau_1 + \tau_2$$

The initial conditions:

$$\begin{cases} t_i(r, \tau_1) = \varphi_i(r, \tau_1), & 0 \leq r < R_i \\ Z_m(\tau_1 + \tau_2) = R_i \end{cases} \quad (5)$$

where $\varphi_i(r, \tau_1 + \tau_2)$, a solution to the problem of heat conduction material inoculator at $\tau = \tau_1 + \tau_2$.

Three period ends when the shell melts completely melt, formed on the surface of the body. Duration of the third period – τ_3 .

Process melting material inoculator begins after heating its surface to the melting point. Thus, we solve the problem of heat conduction for a body with III kind boundary conditions at the outer edge ($r = Z_i$) for calculated area. Heating the body surface is described by the heat equation for the material inoculator at $\tau > \tau_1 + \tau_2 + \tau_2$:

$$c_i(t) \rho_i(t) \frac{\partial t_i(r, \tau)}{\partial \tau} = \frac{1}{r} \frac{\partial}{\partial r} \left[r \lambda_i(t) \frac{\partial t_i(r, \tau)}{\partial r} \right], \quad 0 \leq r < Z_i \quad (6)$$

Boundary conditions at $\tau > \tau_1 + \tau_2 + \tau_2$:

on the axis of symmetry inoculator ($r = 0$) symmetry conditions:

$$\frac{\partial t_i(0, \tau)}{\partial r} = 0 \quad (7)$$

of heat exchange condition on the boundary surface inoculator – melt ($r = Z_k$):

$$\lambda_i(t) \frac{\partial t_i(Z_i, \tau)}{\partial r} = \alpha_m [t_p(\tau) - t_i(Z_i, \tau)] \quad (8)$$

The initial conditions:

$$\begin{cases} t_i(r, \tau_1 + \tau_2 + \tau_3) = \varphi_i(r, \tau_1 + \tau_2 + \tau_3), & 0 \leq r < Z_i \\ Z_i(\tau_1 + \tau_2 + \tau_3) = R_i \end{cases} \quad (9)$$

where $\varphi_i(r, \tau_1 + \tau_2 + \tau_3)$ solution to the problem of heat conduction material inoculator described in period 3, at $\tau = \tau_1 + \tau_2 + \tau_3$. The duration of heating of the body surface to the melting point - τ_4^n .

After heating the surface of the body begins the process of melting, which is described by the heat equation for material ingot (6) at $\tau > \tau_1 + \tau_2 + \tau_3 + \tau_4^n$.

Conditions on the boundary of heat exchange surface of the body - melt ($r = Z_i$):

$$-\rho_i(t)Q_i \frac{dZ_i(\tau)}{d\tau} = \alpha_m(t_p(\tau) - t_L^i) - \lambda_i(t) \frac{\partial t_i(Z_i(\tau), \tau)}{\partial r} \tag{10}$$

$$t_i(Z_i(\tau), \tau) = t_L^i, \quad 0 \leq Z_i < R_i, \quad \tau > \tau_1 + \tau_2 + \tau_3 + \tau_4^n$$

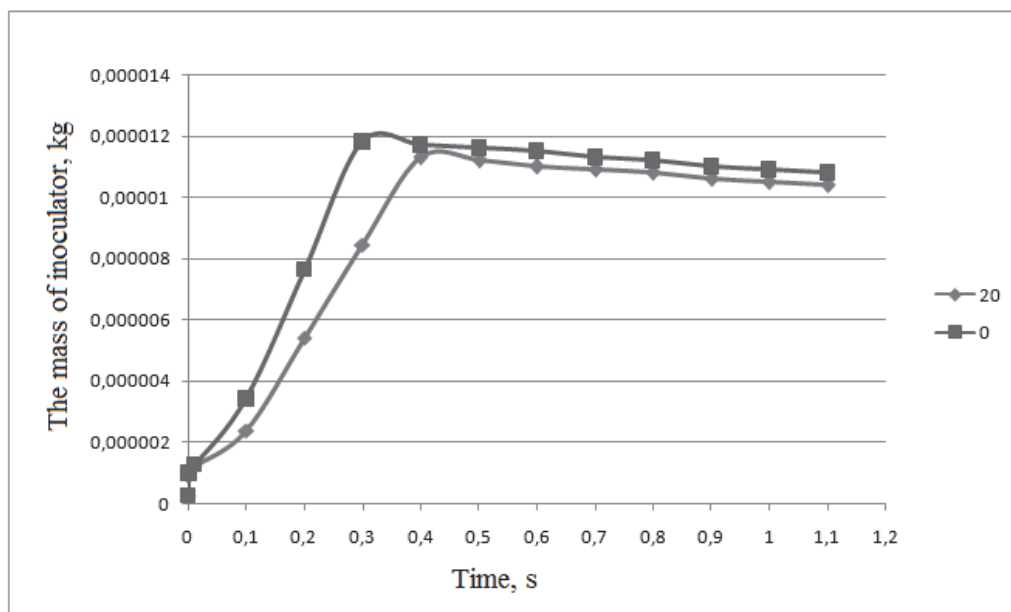
The initial conditions:

$$t_i(r, \tau_1 + \tau_2 + \tau_3 + \tau_4^n) = \varphi_i(r, \tau_1 + \tau_2 + \tau_3 + \tau_4^n), \quad 0 \leq r < Z_i \tag{11}$$

where $\varphi_i(r, \tau_1 + \tau_2 + \tau_3 + \tau_4^n)$, a solution to the problem of heat conduction material inoculator described in the heating period surface of the material inoculator to the melting point at $\tau = \tau_1 + \tau_2 + \tau_3 + \tau_4^n$. The duration of the melting material body - τ_4^{nl} .

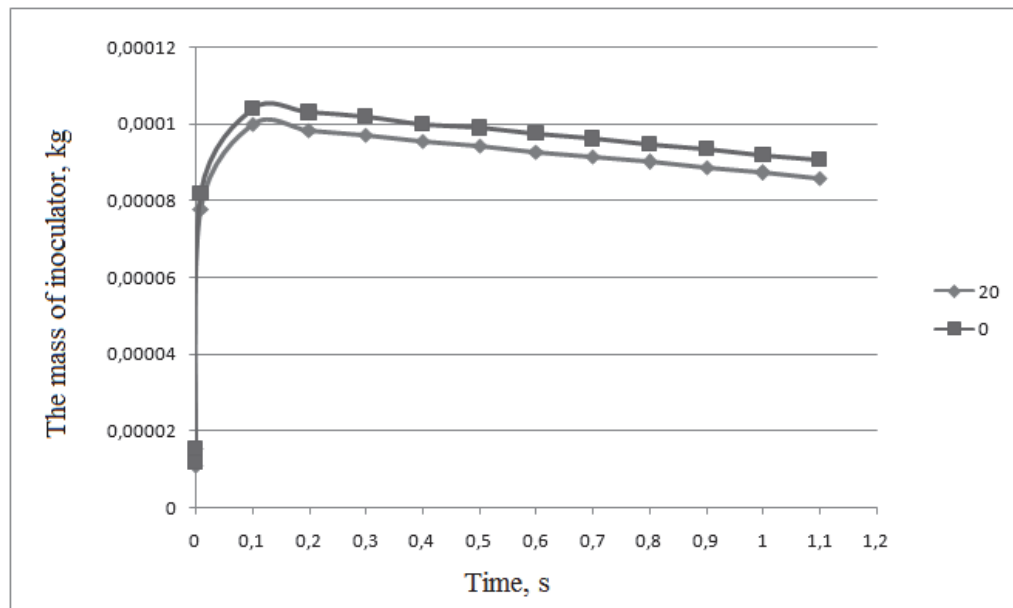
Four periods considered complete with the full melt material inoculator. The duration of the fourth period - $\tau_4 = \tau_4^n + \tau_4^{nl}$.

The estimated model was made using the programming language BASIC, calculations obtained allowed to determine the impact inoculator on the degree of amorphization structure. The calculation results in graphs in figures 1-2. As a model alloy was chosen alloy that has a good tendency to amorphization due content in the element prone to amorphization, Zr [2-3]. In table 1 are researched thermophysical properties of the alloy.



0 - 20 - initial temperature inoculator according 0°C and 20°C

FIGURE 1. Graph changes mass of the alloy $Cu_{45}Ti_{35}Zr_{20}$ in the melting liquid alloy during the initial diameter of inoculator 1 mm



0 – 20 – initial temperature inoculator according 0°C and 20°C

FIGURE 2. Graph changes mass of the alloy $Cu_{45}Ti_{35}Zr_{20}$ in the melting liquid alloy during the initial diameter of inoculator 2 mm

TABLE 1. Thermophysical properties investigated alloy

Alloy	The melting temperature, °C	The transition temperature in amorphous state, K	Density of the alloy, kg/m ³	The heat capacity of alloy, J/(kg·K)	Coefficient of thermal conductivity, W/m·K
$Cu_{45}Ti_{35}Zr_{20}$	1090	410	6900	513.9	175

Conclusion

1. Add inoculator leads to the implementation of the internal heat removal and the formation of additional active melt crystallization centers.
2. Impact inoculator manifested in the increasing speed and preferably volume solidification. This technology differs mainly the implementation of internal heat removal by means of local heat removal.
3. At the time of solid particles inoculator contact with liquid metal melt creates local thermal hypothermia even in the event of significant overheating of total melt.

References

- [1] Pavlenko A.M., Usenko B.O., Koshlak H.V.: *Analysis of thermal peculiarities of alloying with special properties*, Metallurgical and Mining Industry, No. 2, 2014, pp. 15-20.
- [2] Pavlenko A.M., Usenko B.O., Koshlak H.V.: *Mathematical modeling of the casting process in Comsol 3.5a package*, Metallurgical and Mining Industry, No. 1, 2015, pp. 132-140.
- [3] Pavlenko A.M., Usenko B.O.: *Investigation thermophysical processes obtaining of massive amorphous structure*, The special aspects energy and resource saving, Oradea University Press, 2015, pp. 235-274.

THERMAL INSULATION MATERIALS WITH POROUS STRUCTURE

Abstract. *The raw mix of silica-containing technogenic component – fly ash of thermal power plants – and the methods of preparing waterproof porous thermal insulating materials of extended application on its base according to the powder low-temperature technology has been developed using multifunctional properties of soluble glass as: a) a binding component; b) blowing agent; c) the raw mix hardening rate regulator. The physical and chemical, technological aspects of obtaining and using the suggested alkaline-silicate compositions have been considered.*

Keywords: *fly ash, soluble glass, alkaline-silicate composite heat-insulating materials, thermal foaming*

Statement of the problem

Alkali-silicate porous materials obtained by means of thermal or cold foaming of alkali metals silicates aqueous solutions (soluble glass) or solid alkali silicate hydrogels [1-5], are referred to the present-day, efficient inorganic insulants, promising due to the ability to achieve low values of the relative density and thermal conductivity while maintaining sufficient structure strength and easy handling of foaming and induration processes within a wide range of composition formulations. The above benefits are based on the equilibrium and homogeneity of the main raw mixture component: soluble glass and hydrogels based on it.

Composite alkaline-silicate porous thermal-insulating materials, both granulated and block-type, contain significant amounts of the gas phase. There are various technological approaches to obtaining such materials at gas development directly in the strata of the formed composition. Moreover, the process of gas development at high temperatures can be based both on the special additives reactions, and on the crystallization and chemically bound water vapors liberation.

Recent research analysis

To manufacture foam glass, special gas forming agents are used. Normally, the process of making the foam glass lies in preparing the batch, consisting of 95-97% of powdered glass and 5-3% of the gas forming agents (carbonate, such as limestone, or carbon, such as charcoal, coke, carbon dust), heating the batch to the temperature of silicates' pyroplastic state. At this temperature glass grains are sintered and gases formed as a result of the gas-forming agents decomposition, blow highly viscous glass melt. After annealing and cooling, porous material is formed with high thermal insulation properties and high mechanical strength [6]. General issues to obtain the foam glass, including granular one, are described in monographs [7, 8]. The foaming temperature of foam glass usually lies between 750°C and 900°C.

Another method is the heat processing of glassy silicates containing water, which gasifies at high temperatures and foams the silicate base. Raw material in this process can be both natural [9] and synthetic water-containing materials.

To obtain blocks of heat-insulating material, the granular thermal insulating silicate filler can be used, as suggested by the authors [10]. In this case, the use of a silicate binding component permits forming blocks of the required size and shape, and dehydration of the latter occurs at temperatures within 100-350°C.

The feed silicate composition can be obtained by artificial means. In this case, it is often possible to avoid energy-intensive and technologically costly operation of obtaining highly dispersed silicate powders. The raw materials basis for such technical solutions, are water soluble silicates, most frequently sodium silicates. Obtaining of sodium silicates solutions is performed in compliance with the schemes of the technical product synthesis: soluble glass, or by means of silicon oxide dissolution in a strong caustic, or by autoclave dissolution of pre-fused silicate (silicate-blocks). Further, aqueous solution of sodium silicate in one way or another is converted into a gel, for example by adding acids or strong electrolytes, and the resulting material is accessible to heat treatment, when water is removed from it and the product foams, increasing its volume significantly. In this case, if heat treatment of the material is performed in a rigid metal form, then while foaming, the material fills the entire free volume of the form, forming blocks of the given configuration.

Amorphous silica is frequently used to produce sodium silicate with the required $\text{Na}_2\text{O}/\text{SiO}_2$ ratio. Normally, microsilica-wastes from the production of crystalline silicon are used for these purposes [11].

Another option to obtain light porous silicate blocks is mixing the finished granulated lightweight silicate with any binding material, followed by hardening of the composition and obtaining the required blocks. Both of the described approaches to obtaining light silicates have been implemented in numerous technical solutions. At the same time, examples of the particular lightweight products manufacture may have some differences both in the composition of the starting materials and in their processing technology.

As it was noted above, one of the ways to obtain foamed silicate in the form of blocks or slabs is heat treatment in rigid forms of sodium silicates pre-transformed into the gel state with various additives.

For the raw material transformation from the fluid to the thickened pasty state and the subsequent granulation, it is possible to add not only the hydrophobic agent, but also the acidic components to it. Thus, in [12], the option of adding boric acid is suggested. In [13], it is suggested to increase the content of acid oxides in the composition due to adding not only mineral acid, but dispersed acid oxides as well, preferably SiO_2 and Al_2O_3 , due to adding burnt clay: naturally burnt clay (which constituents content is close to that of the TPP fly ash); in [14] – fly ash of thermal power plants is directly suggested.

Modification of additives to soluble glass is also proposed in the study [15]. In the invention described, soluble glass is mixed with portland cement and sodium hexafluorosilicate. The resulting mass is poured into the forms and undergoes heat treatment in the furnace, where the raw mass is additionally blown up and acquires the necessary properties.

Currently, the two technologies for thermal insulating materials manufacturing of rare-glass compositions are suggested. The main difference between them is the method of the starting rare-glass composition preparation. These are process flow diagrams with the use of liquid [16] and mechanical granulation. The both technologies are two-staged and include stages of the prepared rare-glass composition granulation and the subsequent granules heating in a closed form at the temperatures within 400-450°C.

With the use of technologies for liquid granulation of composite systems, there arise difficulties connected with the large fillers granulation, which are difficult to pass through the bushing openings; with maintaining the necessary concentration of Al, Ca, Mg chlorides solutions and their mixtures in the operation cycle and with the worked-out brine utilization.

The indicated problems do not occur while using mechanical granulation, it is possible to use standard equipment. At the moment, the processing technical procedure, which includes mechanical granulation, is the most processable, promising and used in our suggested developments.

An interesting technical solution of the set assignment is the suggested variant of using the starting raw materials mix and the technology used in the production of alkaline-silicate insulation material: "aerated glass" TOV "Stroyevolutsia" [17]. Under its regulations, heat treatment of the soluble glass mixture, a creaming agent (slightly hydrated sodium silicate) and hydrophobe agents are provided. The process of obtaining a granulated "aerated glass" includes homogenizing by mixing the components of the above starting mixture and subsequent heat treatment at 110-115°C. In the course of the transformation, the mass viscosity is significantly growing and the initial liquid system is transformed into a plastic-solid mass. Cooled to the room temperature, the product is completely solidified and acquires fragility, necessary for the subsequent crushing into pieces. After crushing, it is fractionated and "beads" are obtained. The air-entrainment to such "beads" is performed in a boiling layer or in a drum oven at 350-600°C.

The use of such a procedure causes a number of technological problems connected with rheological and environmental difficulties of introducing in this way hydrophobe agents into the composite system, with the possibility to reproduce the dimensions and regularity of pores, the granules macrostructure strength in general and the reduction of internal tension in the products.

Identification of previously unsettled parts of the general problem

Analysis of the existing suggested raw mixtures formulations and methods of obtaining thermal insulating materials proves that introducing a significant gel formers amount has a serious drawback: the gelling agent breaks the soluble glass structure to form hydrosilicic acid gel, which is capable of retaining less water than soluble glass. This adversely affects the porosity of the resulting rare glass compositions. Therefore, there is a need to introduce such substances that are inert to soluble glass at the normal temperature.

In addition, a significant drawback of the known methods is performing air-entrainment at fixed temperatures in the furnace within the range of 300-700°C. Such a mode of heat treatment reveals several contradictory trends.

At relatively low temperatures, the air-entrainment process is complicated due to the low warming-up rate of the raw mass internal areas, resulting in the increased duration of its air-entrainment process.

At the same time, the slow warming up of rare-glass mixtures also leads to significant losses of chemically bound water, due to which air-entrainment of the mixtures occurs. The high rate and unevenness of their heating is manifested in the size, regularity of the pores and the strength of the entire porous structure, in the internal tensions of the products. Therefore, an important prerequisite for obtaining the expanded material possessing a set of required properties and their reproduction, is compliance with the principle of correspondence between the rate of crystallization and chemically bound water isolation and the rate of new solid silicate structures formation.

In all of the above-described methods, the first stage is to obtain a solid or plastic composition from soluble glass which can then be subjected to heat treatment. At the same time it is not necessary to use different additives that cause coagulation of silicates. It is possible to obtain a plastic composition using soluble glass simply by means of adding an inert disperse component.

Statement of assignment and methods of its solving

The study performed is aimed at the search and development of an optimized raw material mixture variant of the silicon oxide containing technogenic component: fly ash of thermal power plants and methods of obtaining the fly ash based porous alkaline-silicate composite thermal insulating materials of extended application, differing from the analogues by their composition, the content of the starting raw mass, the sequence and modes of the target product formation, the applied technological equipment.

Study results and their discussion

In the present project, the set task of making the targeted porous thermal insulating material is achieved by means of the raw mass hot foaming technology, which procedure includes the four main stages:

- 1) preparation of the starting raw mixture components and homogenization of the latter;
- 2) the composite system “gaging” by soluble glass and formation of a persistent gel; fragmentation of the hardened raw mass and placement of the granulate into lined dismountable molds;
- 3) heating and transferring of the workpieces’ substance into the pyroplastic state (110-115°C);
- 4) further hot foaming and reproduction of the regular porous macrostructure of composite systems (130-220°C) and formation of the targeted processed product’s properties (500-550°C).

The blowing agent in this case is water (mainly silanol or molecular, strongly bound by hydrogen bonds with unbridged oxygen atoms), which is released during heat treatment of composite systems.

In the raw mixture, the industrial soluble glass, thermal power plants fly ash of the mixed chemical composition (see table 1), sticky portland cement and, additionally, a thickener (pre-staged partially dehydrated hardened “dry glass”) are used.

TABLE 1. Chemical composition of the thermal power plants fly ash, mass. %

SiO ₂	Al ₂ O ₃	Fe ₂ O ₃	MgO	CaO	Na ₂ O	K ₂ O	Mn ₃ O ₄	TiO ₂	SO ₃	P ₂ O ₅
51.68	16.75	14.47	0.88	4.38	0.35	2.58	0.04	0.86	4.24	0.49

In the prepared samples, the fly ash provides good reinforcing properties, high thermal stability, sufficient resistance to aggressive media, has a small bulk density.

At the same time, the results of the authors’ studies [18, 19] (on the ability of alkaline-silicate systems with Al₂O₃ in alkaline media to form insoluble products of Na₂O·Al₂O₃·2Si₂O₃·nH₂O) permit to consider aluminum oxide contained in ash to be a modifying component that provides the raw mix with the properties necessary for the targeted product formation.

In forming the raw mix, the results were taken into account on improving the water resistance of alkali silicate composition by means of replacing the two-calcium silicate (belit) hydrophobe components with the sticky Portland cement; the results are presented in [20].

The “setting” rate control of the suggested raw mix during the formation of hydrosilicic acid xerogel (depending on the executed tasks purposes) was performed by means of varying properties of the thickener used and by means of regulating the hardened processed mass fragmentation in the further processes and its subsequent hot foaming.

The raw mix prepared according to the optimized formulation, in contrast to the previously considered analogues, starts hardening at the usual temperature from the moment of its “gaging” with soluble glass and forms a plastic cake with the properties necessary for further fragmentation.

The suggested raw mix also permits to overcome the difficulties associated with drying of viscous rare-glass mix to remove a large output amount of water (56-62%) to the water content of 33-38% needed to obtain a rigid hydrogel capable of thermal blowing.

The optimized formulation of the raw mix allows processing of the compositions in various ways, with the formation of thermal insulating materials of extended application. An important prerequisite for their reproduction with the necessary properties system is strict compliance with the regulatory requirements established by the previous empirical studies.

In parallel with the formulation development, the technology of samples manufacturing was being tried. Thereat, the decisive factor, in contrast to the regulations [17], the exclusion of the raw mix granulation stage after heat treatment 110-115°C and the use of sealed closed forms at their temperature annealing.

The suggested hot air entrainment of the silicate compositions structure “blowing” of the systems in a xerogel form passes quickly, avoiding the viscous-adhesive state. The determining factor in the process of the systems thermal activation was the technical performing of their heating reproduced rate [see 21].

The conscious choice of its optimal mode is motivated by empirical data to determine the thermal foaming features of composite systems obtained by the method of differential-thermal analysis (DTA) presented in figure 1.

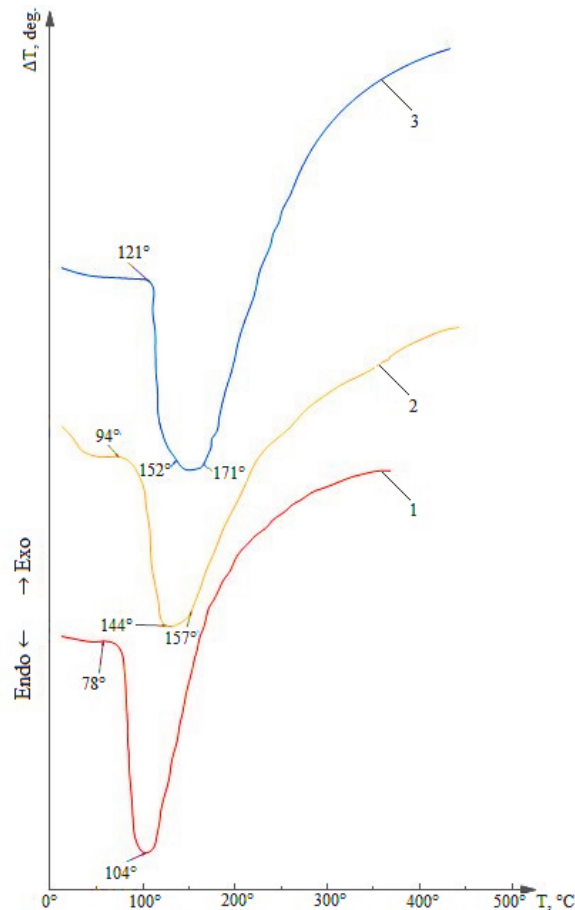


FIGURE 1. DTA thermograms of sodium rare-glass composites xerogels in coordinates $\Delta T - T$, recorded at heating the samples in adequate conditions at different rates: curve 1 – 4 deg./min, curve 2 – 7 deg./min, curve 3 – 20 deg./min

The air entrainment process includes three main stages, the duration and nature of which depend on the type and amount of water containing the raw mix:

- within the range of 100-110°C, the hardened composite system partially transforms into the pseudopyroplastic state and begins to deform with increasing volume;
- within the range of 130-147°C, an intensive release of free and adsorbed water and intensive air entrainment of the sample mass occurs;
- at the temperature values above 147°C, the removal of constitutional moisture, the completion of restructuring, physical and chemical transformations of composite systems are observed.

Based on the analysis of the thermographic data and the macrostructure of the samples obtained, it can be concluded that the greatest contribution to the formation of the product’s structure with maximum homogeneity is made by the constitutional water, while removal of the excess adsorption moisture at the initial stages leads to the formation of large through pores and capillary channels in the raw mass. Therefore, the initial rare-glass composition should contain a minimum amount of free and adsorbed water.

As the efficient ways to reduce the free water's effects, the following ones can be recommended:

- direct thermal dehydration and transformation of soluble glass into xerogel (the basis of the present variant of the suggested technical solution);
- liquid granulation of composite systems (for example, in Al, Ca, Zn, Mg chlorides solutions or their mixtures);
- introducing of mineral fillers or chemical additives into the rare-glass composite system, which leads to the development of gelation processes.

According to the results of the study [22], alkaline-silicate compositions in solutions at heating form a number of hydrated associates with differing properties (see fig. 2). This permits modifying the properties of the raw mix thickener – grated “dry glass” – by means of the partial unwatering of the purchased product in a liquid state at different temperature values, in the conditions of the technological cycle for the target product formation, simultaneously with the same equipment, without the use of additional equipment. Meanwhile, the empirically determined physicochemical behavior of composite silicate systems, the features of unwatering and the viscosity state passing, strong adhesion of the intermediate transformation products to metals, ceramics, glass allow to suggest technological regulations, stages, sequence of operations during processing, development and selection of the equipment materials, variations in the methods of obtaining and using porous targeted composites.

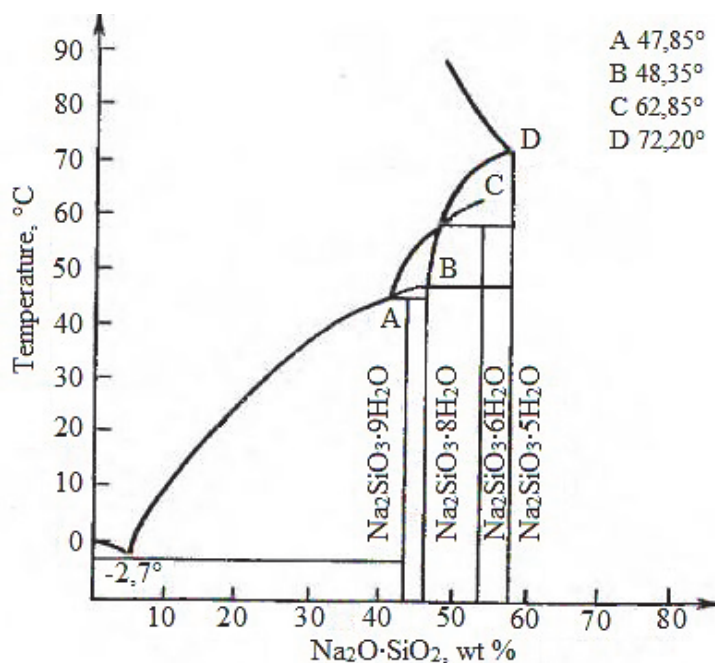


FIGURE 2. Solubility in the $\text{Na}_2\text{O} - \text{SiO}_2 - \text{H}_2\text{O}$ system

Laboratory practice proves that the excess amount of the soluble glass introduced in a liquid state during the “gaging”, on the one hand improves the rheological properties, the plasticity of the treated raw mix, and on the other hand, during the subsequent heat treatment, causes additional viscosity of the system, deteriorates the heat transfer conditions, requires more prolonged temperature holding at higher temperature values and leads to the increased energy costs. Therefore, a necessity arises to find an efficient way of regulating the rate of gelling, using the method of shifting the equilibrium of physical and chemical processes of the disperse systems dehydration by adding less hydrated forms of the dried soluble glass; with the degree of the grated “dry glass” dispersion, with its dosage and regulating the processes of the hardened processed mix fragmentation during the granulate formation and the subsequent hot air entrainment.

The improved formulation of the raw mix preparing allows processing compositions in various ways with the formation of insulating materials of extended application: granular insulating filler (fig. 3),

materials for thermal insulation for the structures complicated in the form (fig. 4), the plate and film-like types of insulating materials (fig. 5). This task (depending on the purpose and features of the performed tasks) is solved by the capability of performing the final stages by means of several different ways of the products obtaining.

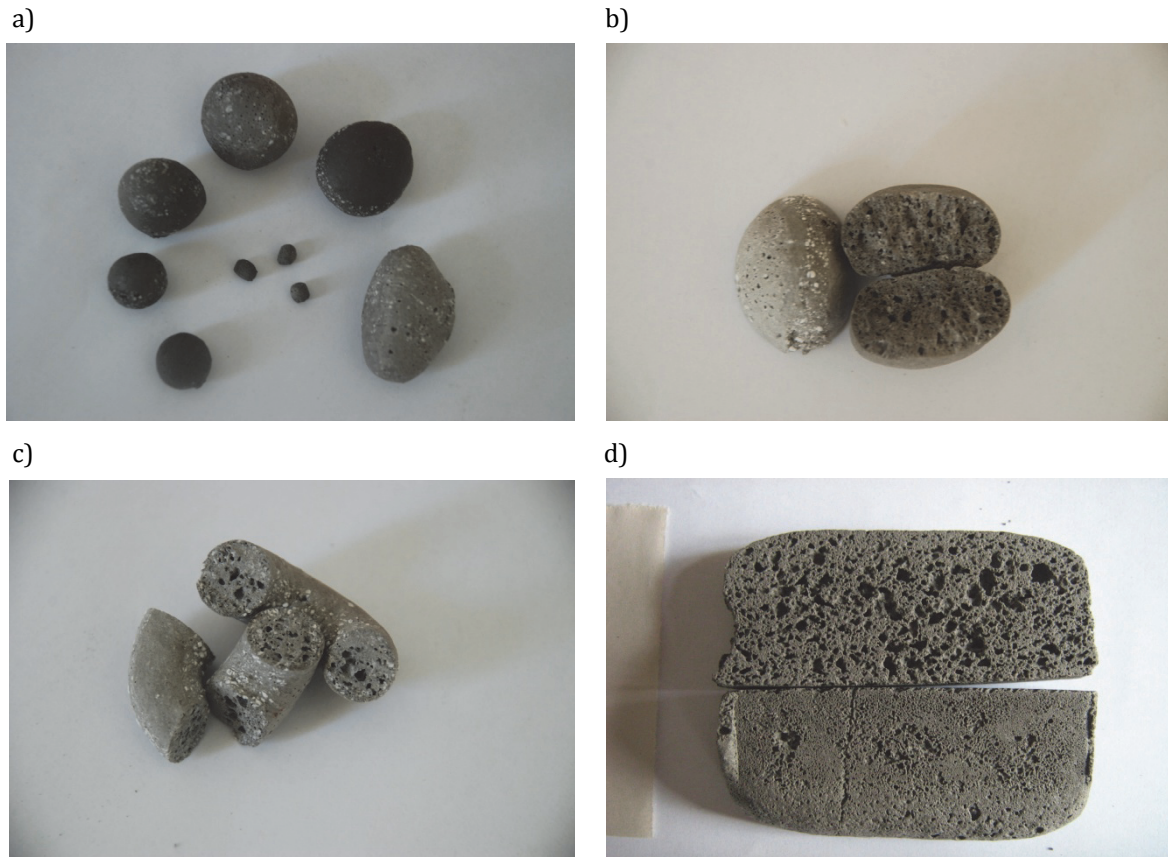


FIGURE 3. Illustration of the granular thermal insulating fillers' samples, obtained in the lined molds without limitation of formation volume: a), b) cutting of iso-sized elements; c) cutting elements of plastic hardened raw cake of the set preformed thickness; d) of workpieces, formed in separate dismountable molds

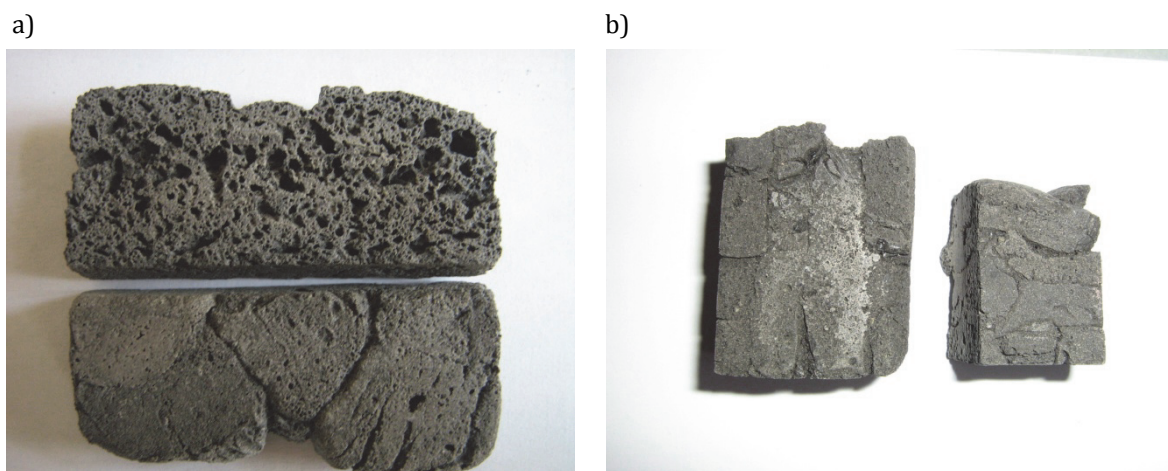


FIGURE 4. Illustration of fragments of thermal insulation zones sections in complicated form structures performed by the working zone filling with fragmented elements and the subsequent heat treatment in dismountable equipment of varying complexity: a) without limiting the free volume of formation; b) with restriction of formation space

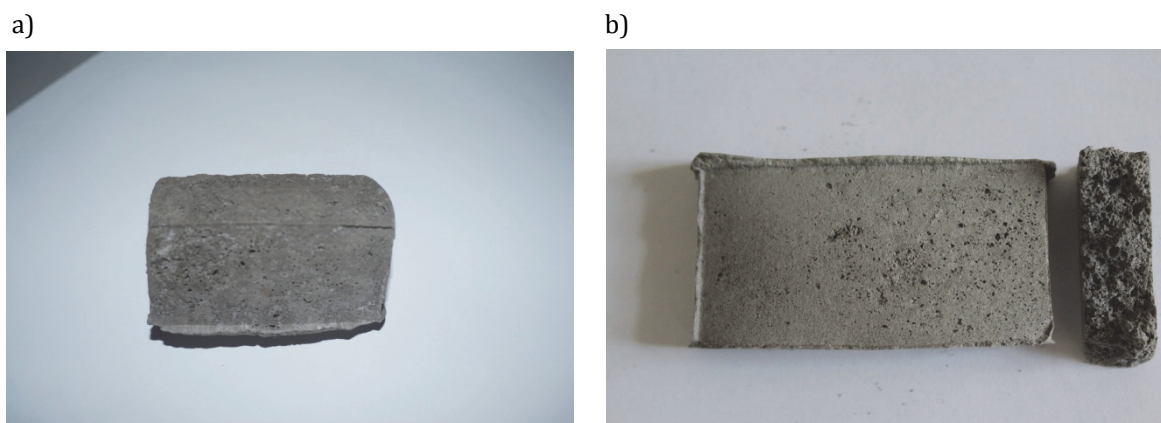


FIGURE 5. Illustration of the items fragments formed: a) in the form of plates; b) in the form of films

The use of the two stages procedure of the suggested renovation in the technology of preparing the porous thermal insulating materials determines: 1) the nature and the behavior peculiarities of the rare-glass composite systems components during the heat treatment, their strong adhesion manifestation related to most structural materials; 2) the necessity to solve the problem of easy workpieces removal from the formation molds; 3) the choice of the method for lining the internal surfaces of dismountable equipment molds; 4) thermophysical and chemical properties of the used lining material.

The features of the suggested project are:

- ease and availability of obtaining components and preparing the raw mix;
- formation of the raw mix directly at its “gaging” with soluble glass under the normal conditions;
- the thermal insulation method is fast;
- the possibility of easy formation and fragmentation of the raw workpieces, their inherent properties makes it possible to spread in time and space separate stages of thermal insulation: the stage of preparation, formation of granulate (possibly, in a specialized site); storage; transportation; technological packing in the working area complying with the increased resistance requirements to the heat transfer (possibly, in the construction site);
- processing of complicated working areas: selection of the raw mix cake thickness, the size and shape of the starting fragmented elements (depending on the target task and in order to provide more tight packing);
- the versatility of the thermal insulation method (based on the manifestation of significant adhesion ability of alkaline-silicate composite systems in relation to most structural materials: metals, ceramics, glass, wood);
- low shrinkage with the suggested formulation of the raw mix and the method of treatment;
- indifference to most components and stability of the thermal insulation material properties, high thermal and chemical resistance, non-combustibility, ability to withstand significant temperatures;
- combination of the valuable properties set: low thermal conductivity factor, thermal stability, incombustibility, durability, low cost.

Conclusions

The raw mix of silica-containing technogenic component – fly ash of thermal power plants – and the methods of preparing waterproof porous thermal insulating materials of extended application on its base according to the powder low-temperature technology has been developed using multifunctional properties of soluble glass as: a) a binding component; b) blowing agent; c) the raw mix hardening rate

regulator. The physical and chemical, technological aspects of obtaining and using the suggested alkaline-silicate compositions have been considered.

References

- [1] Pavlenko A., Koshlak H.: *Production of porous material with projected thermophysical characteristics*. Metallurgical and Mining Industry, No. 1, 2015, pp. 123-127.
- [2] Malyavsky N.I.: *Shchelochno-silikatnyie utepliteli. Svoistva I khimicheskiye osnovy proizvodstva* [Alkaline silicate heat insulants. Properties and chemical bases of production], N.I. Maliavsky, Rossiyskiy khimicheskiy zhurnal – Russian Chemical Journal (Zh. Ros. khim. ob-va im. D.I. Mendeleeva – Journ. of D.I. Mendeleev Russian Chemical Society)], 2003, V. XLVII, No. 4, pp. 39-45.
- [3] Leonovich S.N.: *Osobennosti polucheniya Shchelochno-silikatnykh teplozoliatsionnykh materialov* [Features of obtaining alkaline-silicate heat-insulating materials], S.N. Leonovich, G.L. Shchukin, A.L. Belanovich et al., Nauka i tekhnika [Science and Technology], 2012, No. 6, pp. 45-50 (in Byelorussia).
- [4] Figovskiy O.L.: *Zhydkoye steklo i vodnyie rastvory silikatov kak perspektivnaya osnova tekhnologicheskikh protsessov polucheniya novykh nanokompozitsionnykh materialov* [Soluble glass and aqueous solutions of silicates as a promising basis for the technological processes of obtaining new nanocomposite materials] O.L. Figovskiy, P.G. Kudryavtsev, Elektronnyi nauchnyi zhurnal: Inzhenernyi vestnik Dona. [Electronic scientific journal: Engineering bulletin of Don.], 2014, Vol. 29, No. 2, Doc. 2448, pp. 55-97.
- [5] SHI F., WANG L., LIU J., ZENG M.: *Effect of heat treatment on silica aerogels prepared via ambient drying*, J. Mater. Sci. Technol., 2007, Vol. 23, No. 3. pp. 402-406 (in Chinese).
- [6] Pavlenko A., Koshlak H.: *Design of processes of thermal bloating of silicates*. Metallurgical and Mining Industry, 2015, No. 1, pp. 118-122.
- [7] Pavlenko A.M., Koshlak H.V., Piotrowski J.Z.: *Determination of heat transfer coefficient in the phase-change heat storage device*. Structure and Environment, 2016, No. 4, pp. 278-281.
- [8] Koshlak H.V., Pavlenko A., Piotrowski J.Z.: *The energy parameters of formation of the porous structure*. Structure and Environment 8 (3), pp. 206-210.
- [9] Pavlenko A.: *Dimensions of the nucleus agent pore former closed spherical pores*. A. Pavlenko, H. Koshlak, Aktualne zagadnienia energetyki, budownictwa i inżynierii środowiska, Koszalin 2016, pp. 75-83.
- [10] Patent of the Russian Federation No. 2161142, IPC (International Patent Classification) C04B 28/24. Sposob polucheniya teplozoliatsionno-konstruktsionnogo materiala na osnove vspuchennogo vermikulita [Method of obtaining heat-insulating construction material based on expanded vermiculite]. A.V. Pariy, N.S. Nikonova, E.A. Bazhanov – Claimed on June 6, 2000 – Published on 27.12.2000.
- [11] Patent of the Russian Federation No. 2097362, IPC C04B 38/00. Syryevaya smes dlia polucheniya penosilikatnogo teplozoliatsionnogo materiala [Raw mix for obtaining foam-silicate insulation material] N.F. Artemenko, V.I. Golubev, S.D. Bondar, R.F. Valeyev, S.V. Malofeyev, V.N. Shevelev, M.M. Mubarakshin, G.K. Mardamshin – Claimed on May 17, 1995 – Published on November 27, 1997.
- [12] Patent of the Russian Federation No. 2220927, IPC C04 B 28/26. Syryevaya smes i sposob polucheniya granulirovannogo teplozoliatsionnogo materiala [Raw material mix and method of obtaining a granulated heat-insulating material] T.N. Radina, M.Yu. Ivanov – Claimed on April 19, 2002 – Published on 01.10.2004.
- [13] Patent of the Russian Federation No. 2220928, IPC C04B 28/26. Syryevaya smes i sposob polucheniya granulirovannogo teplozoliatsionnogo materiala [Raw material mix and method of obtaining a granulated heat-insulating material] T.N. Radina, M.Yu. Ivanov – Claimed on April 29, 2002 – Published on 01.10.2004.
- [14] Patent of the Russian Federation No. 2246463, IPC C04B 28/26. Syryevaya smes i sposob polucheniya zernistogo teplozoliatsionnogo materiala [Raw material mix and method of obtaining a grain heat-insulating material] T.N. Radina, A.I. Kudyakov, M.Yu. Ivanov – Claimed on 22.10.2003. – Published on 20.02.2005.
- [15] Patent of the Russian Federation No. 2134668, IPC C04B 28/26. Sposob izgotovleniya poristykh silikatnykh materialov [Method for manufacturing porous silicate materials] S.I. Brykov, V.M. Busygin, R.G. Valeyev, L.G.

- Reisin, K.S. Galimov, F.A. Zakirov, V.I. Korneyev, N.A. Mochalov, I.H. Mukhametov, Yu.A. Poddubnyi, T.D. Tikhonova, A.A. Fedurin – Claimed on May 29, 1998 – Published on 08.20.1999.
- [16] Patent of the Russian Federation No. 2268248 (13), IPC C04B 38/00. Vspenennyi material i sposob yego izgotovleniya [Foam material and the method of its manufacture] V.A. Lotov, K.A. Rudik – Claimed on July 06, 2004 – Published on January 20, 2006.
- [17] Koshlak H.V.: *Use of burshtyn tpp ash for the production of expanded gas concrete*. Energy, energy saving and rational nature use, No. 2 (5), 2016, pp. 87-95.
- [18] Koshlak H.: *Heat exchange in a confined space*. Problem of energy saving and nature use 2013. Budapest 2014, pp. 87-92.
- [19] Ovcharenko G.I.: *Tseolity v stroitelnykh materialakh* [Zeolites in Building Materials] GI I. Ovcharenko, V.L. Sviridov, L.K. Kazantseva. – Barnaul: AltGTU, 2000, 320 p.
- [20] Maliavsky N.I., Zvereva V.V.: *Kaltsiy-silikatnyie otverditeli zhidkogo stekla dlia polucheniya vodostoykikh shchelochno-silikatnykh utepliteley* [Calcium-silicate liquid glass hardeners for obtaining water-resistant alkaline-silicate insulants] ISSN 1994-0351. Internet-vestnik [Internet-bulletin] of the VolgGASU. 2015. Issue 2 (38). www.vestnik.vgasu.ru
- [21] Koshlak H.: *Temperature state plate in conditions convective heat transfer*. A. Pavlenko, H. Koshlak: Collection of scientific articles «Energy, energy saving and rational nature use», Radom: Kazimierz Pułaski University of technology and Humanities in Radom No. 1 (4), 2015, pp. 108-114.
- [22] Koshlak A.: *Solution of equations thermal conductivity*. Collection of scientific articles «Energy, energy saving and rational nature use», Radom: Kazimierz Pułaski University of technology and Humanities in Radom, No. 2 (3), 2014, pp 38-49.

Anastasiia PAVLENKO

Dnieperovskii State University, Ukraine

THERMAL CONDUCTIVITY OF THE GAS IN SMALL SPACE

Abstract: *he article is devoted to research of peculiarities of porous materials with micropores thermal conductivity. The temperature influence pattern of heating surface on the process of heat transfer by convection in the pores is given. Mathematical model of gravitational convection, which allows to predict the intensity of the convection current is proposed.*

Keywords: *convective heat exchange, the particulate material, thermal gradient.*

Convective heat exchange arising in the pores of the material dominates the elementary components of heat exchange in porous materials. That is why theoretical analysis of convective heat transfer is the actual problem, which comes to development a methodology for quantitative evaluation of convective heat transfer in the pores of heterogeneous systems.

Traditional methodology of evaluation the nature of heat transfer in enclosed space is based on the calculated Grashof number (Gr) and Prandtl (Pr) for particular environment.

Correlation of these numbers in a given range of values makes it possible to establish the presence of convection currents in the heated surface. One may judge about the accuracy of such assessment from the change of intensity of heat transfer under the conditions of heat conditions change. Such qualitative characteristic of heat transport process in our view does not reflect real physical processes occurring in confined space. The intensity of gravitational convection current is determined not only by thermophysical characteristics of contacting media, scaling factors, but also by orientation of the heating surface in space. Heat is transferred from the surface in the near-wall region, the thickness of which is sufficiently small. If one takes it as a scale factor for Grashof's equation, the number of Gr will not exceed the critical value corresponding to a heat transfer conduction. But when heating the space through the side surfaces the convection currents are always present. And the question of what they contribute to the heat transfer remains relevant.

The figure 1 shows that along the walls of the layers with relatively high flow rate are forming. Isolines in the center tend to a horizontal position. Such current distribution was more typical for all calculated cases. When large numbers Gr gasflow from the heated surface is formed. It is for these cases in the literature critical numbers Gr are shown, which formalize the heat transfer process in closed area.

But convective heat transfer can occur along the surface, wherein the moving in the center of motion is absent. Such a case in the literature is considered to be the heat transfer by thermal conductivity. Obviously, the energy transfer in the boundary layer can be significant.

To estimate the intensity of heat transfer, mathematical model connecting the surface temperature with the speed of convective current was developed [1].

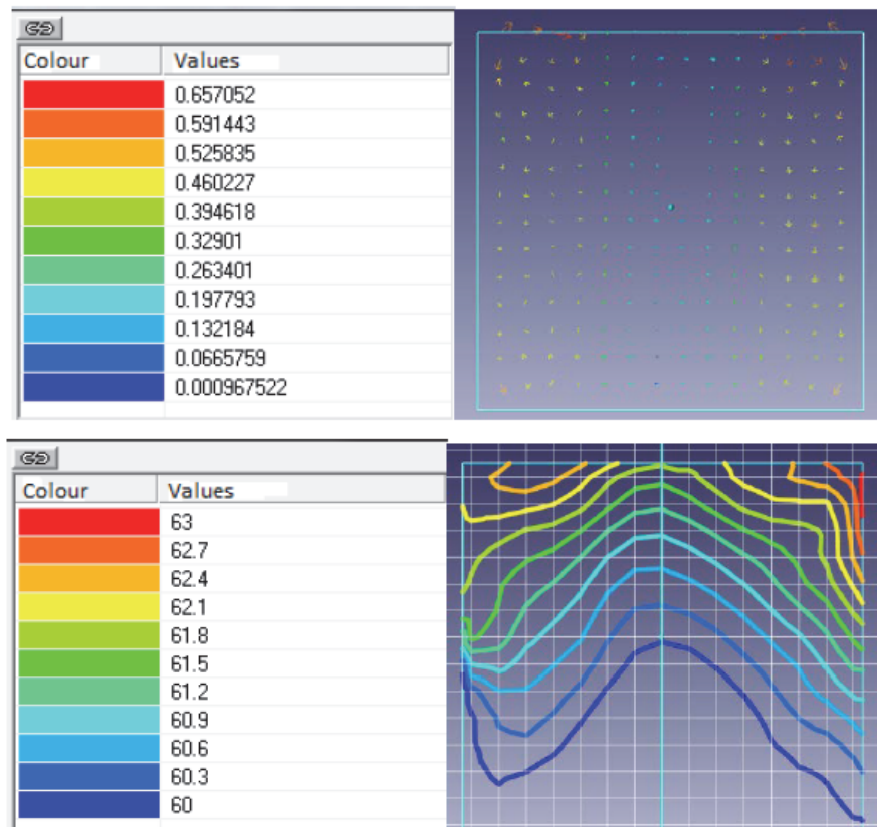


FIGURE 1. Distribution of velocities and temperatures

Mathematical model of gravitational convection includes the following equations:

$$\frac{\partial V}{\partial t} + (V \cdot \nabla)V = -\frac{1}{\rho_0} \nabla p + \nu \nabla^2 V + [1 - \beta(T - T_0)]g \quad (1)$$

$$\nabla \cdot V = 0 \quad (2)$$

$$\frac{\partial T}{\partial t} + V \cdot \nabla T = a \nabla^2 T \quad (3)$$

where:

ν – kinematic viscosity coefficient $\nu = \eta / \rho_0$;

a – thermal diffusivity, values which correspond to the tabular ones for $T = T_0$, $a = \frac{\lambda}{c\rho}$;

V – velocity vector;

p – pressure;

T – absolute gas temperature;

ρ – density;

η – dynamic viscosity;

λ – thermal conductivity;

t – time;

g – acceleration of free fall.

For simplicity we may use the Oberbeck-Boussinesq approximation. T_0 is some value from the interval of temperature change in the medium, at which the density equals. Let us suppose that the temperature T in the medium deviates a little from T_0 . Then the equation of state may be linearized,

leaving only a member of the 1st-order of smallness in the expansion of a function $\rho(T)$ in a Taylor series in the neighborhood of the value T_0 :

$$\rho = \rho_0(1 - \beta(T - T_0))$$

where $\beta = -\frac{1}{\rho_0} \frac{\partial \rho(T)}{\partial T}$ is coefficient of thermal expansion of the gas at $T = T_0$.

Density dependence on the temperature is taken into account only in the term with volume force of gravity ρg , but in other cases they consider $\rho = \rho_0$. Under such assumptions, the problem becomes as follows:

Let us find a solution to the boundary value problem:

$$\lambda \frac{\partial T(r, \theta)}{\partial r} + \alpha T(r, \theta)_{r=R} = f(\theta) \tag{4}$$

For partial differential equations:

$$V \frac{\partial T(r, \theta)}{\partial r} + a \Delta T(r, \theta) \tag{5}$$

here

$$\Delta = \frac{\partial^2}{\partial r^2} + \frac{2}{r} \frac{\partial}{\partial r} + \frac{1}{r^2} \left[\frac{\partial^2}{\partial \theta^2} + ct\theta \frac{\partial}{\partial \theta} \right] \tag{6}$$

here

$$\frac{\partial T^2(r, \theta)}{\partial r^2} + \left(\frac{2}{r} - \frac{V}{a} \right) \frac{\partial T(r, \theta)}{\partial r} + \frac{1}{r^2} \left[\frac{\partial^2 T(r, \theta)}{\partial \theta^2} + ct\theta \frac{\partial T(r, \theta)}{\partial \theta} \right] \tag{7}$$

Approximate solution of the problem for equation (5) becomes:

$$T(r, \theta) \approx R \cdot \exp \left[-\frac{1}{2} \frac{V}{a} (R - r) \right] \sum_{n=0}^{\infty} \frac{f_n \left(\frac{r}{R} \right) P_n(\cos \theta)}{\lambda \left(\frac{1}{2} \frac{V}{a} R + n \right) + \alpha R} \tag{8}$$

Solution of equation (8) is shown in the graph of figure 2.

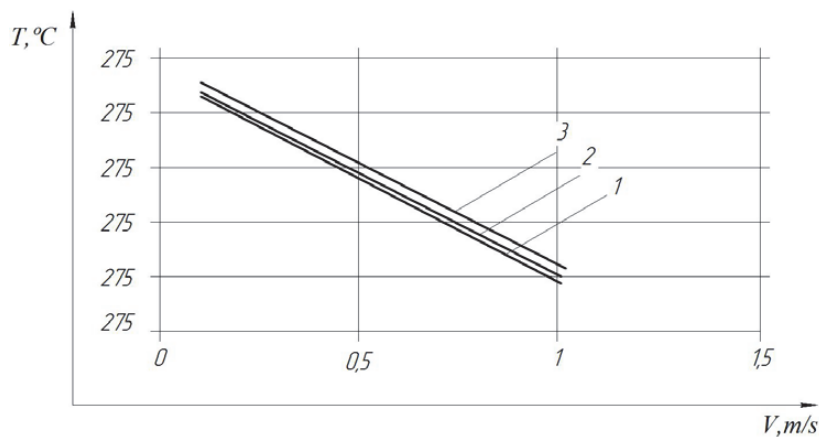


FIGURE 2. The solution of equation (8), where: 1 - the pore radius $r = 2.5$ mm; 2 - the pore radius $r = 4.5$ mm; 3 - the pore radius $r = 7.5$ mm

For vertical heating wall the calculated values of the number $Nu = f(Gr, Pr)$ are given in figure 3.

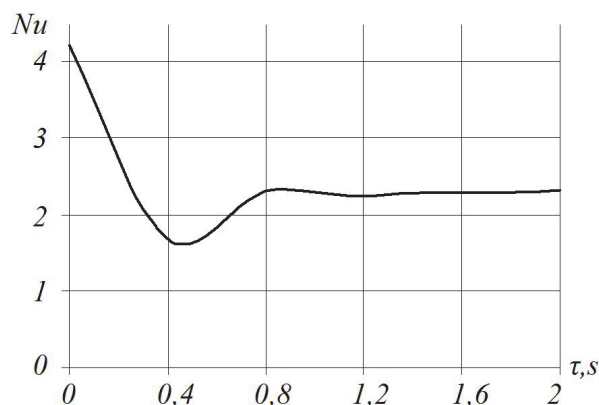


FIGURE 3. Change the number Nu in time for the conditions of the figure 1

Conclusions

The calculations performed confirm the presence of convective current on the heating surface in closed gas volumes with any geometric and energetic characteristics.

According to computation data it is possible to determine the basic stages of heat transfer and set their boundaries. On the graph of figure 3 in the time interval $\tau = 0 - 0.4$ one may observe the relaxation period of gas (air) heat exchange with the surface. If convective heat transfer was absent, meaning of the number would approach to Nu to 1, i.e. heat flux transmitted by convection would be equal to the heat flux thermal conductivity. The minimum value of Nu number on the graph corresponds to the beginning of convective transfer.

Thus, the above mathematical model and calculations allow to perform a quantitative analysis of the convective heat transfer in

dependence on the temperature of the heating surfaces in a closed volume.

References

- [1] Pavlenko A.M., Basok B.I., Avramenko A.A.: *Heat Conduction of a Multi-Layer Disperse Particle of Emulsion*. Heat Transfer Research. 36, (1,2), 2005, pp. 55-61.